ISSN 0386-4049

気象研究所技術報告 第七十一号

TECHNICAL REPORTS OF THE METEOROLOGICAL RESEARCH INSTITUTE No.71

Meteorological Research Institute Ensemble Prediction System (MRI-EPS) for climate research
- Outline and its applications -

BY

Shoukichi Yabu, Ryo Mizuta, Hiromasa Yoshimura, Yuhji Kuroda, and Hitoshi Mukougawa

気象研究所技術報告
第 71 号

気候研究のための気象研究所アンサンブル予測システムの概要とその応用

藪将吉，水田亮，吉村裕正，黒田友二，向川均

気象研究所

METEOROLOGICAL RESEARCH INSTITUTE, JAPAN
March 2014

TECHNICAL REPORTS OF THE MRI, NO.71

The *Technical Reports of the Meteorological Research Institute* has been issued at irregular intervals by the Meteorological Research Institute (MRI) since 1978 as a medium for the publication of technical report including methods, data and results of research, or comprehensive report compiled from published papers. The works described in the *Technical Reports of the MRI* have been performed as part of the research programs of MRI.

Meteorological Research Institute Ensemble Prediction System (MRI-EPS) for climate research
- Outline and its applications -

BY

Shoukichi Yabu[1], Ryo Mizuta[1], Hiromasa Yoshimura[2], Yuhji Kuroda[1], and Hitoshi Mukougawa[3]

[1]Climate Research Department, Meteorological Research Institute

[2]Forecast Research Department, Meteorological Research Institute

[3]Disaster Prevention Research Institute, Kyoto University

気象研究所技術報告

第 71 号

気候研究のための気象研究所アンサンブル予報システム（MRI-EPS）

－概要とその応用－

籔　将吉[1]、　水田　亮[1]、　吉村裕正[2]、　黒田友二[1]、　向川　均[3]

1 気象研究所気候研究部

2 気象研究所予報研究部

3 京都大学　防災研究所

序

全球大気モデルを用いた台風の進路予報や週間から１か月にわたる延長予報、さらに大気海洋結合モデルを用いた季節予報まで、初期値問題に基づく予測可能性やアンサンブル予報の研究が、世界の気象機関や大学・研究機関で広く実施されている。また、数値予報モデルを用いた大気の予測可能性の研究は、単なる気象技術を超えて大気運動の非線形性を捉えた学問的な研究対象としても認識されている。

このような中で、平成17年1月から気象庁地球環境・海洋部と京都大学防災研究所の向川均教授のグループが、共同研究「熱帯域における季節内振動の予測可能性評価」を実施した。この共同研究では、気象庁の１か月予報で採用されている初期摂動作成法であるBGM（Breeding of Growing Mode）法を改良し，日本の天候に大きく影響する熱帯大気の特性を取り入れた初期摂動を得ることに成功した。この成果は平成19年3月に気象庁の１か月予報業務に取り入れられ、熱帯を中心とする予測精度の向上に大きく寄与した。

一方、気象研究所気候研究部の研究者は、向川教授とともに成層圏-対流圏結合系の変動メカニズム解明と関連する延長予報の可能性を、数値モデル実験によって研究してきた。この中で、極夜ジェット振動が卓越した場合には季節予測の予測可能性が大きく高まることを指摘し、季節予報に新たな可能性を示した。この成果をさらに発展させるために、気象研究所と京都大学防災研究所との間で最近、数値予報モデルや気候システムモデルを用いた本格的な予報実験を実施するための共同研究を始めたところである。

しかしながら、気象庁の数値予報システムを直接、大学・研究機関との共同研究で利用しようとする場合、現業数値予報のために効率化された数値予報システムや特殊なデータ形式が、一般研究者による利用の少なからぬ障害となる。そこで気候研究部では、気象庁１か月予報システムを入出力データに自由度を持たせた汎用性のあるプログラムとして整備し、気象研究所アンサンブル予報システム（MRI-EPS）とした。現業１か月予報システムの初期摂動は北半球と熱帯域の成長モードだけを組み合わせているが、MRI-EPSでは初期摂動を南半球に拡張することによって全球の予報実験にも対応できるようにした。

この気象研究所技術報告には、今回開発したBGM法によるMRI-EPSについて、その理論、技術的仕組み、実際の利用法が記述されている。特に数値予報実験を実施する研究者の利用を念頭に丁寧にまとめた報告書になっており、１か月予報や季節予報などの数値予報実験を通して、気象庁・気象研究所と大学・研究機関との共同研究の発展に大いに寄与することを期待している。

気候研究部長

露木　義

Abstract

A new ensemble prediction system has been developed to facilitate climate research in the Meteorological Research Institute (MRI). The system, MRI-EPS (MRI Ensemble Prediction System), has been constructed by expansion of the ensemble forecasting system developed for operational one-month forecasting in the Japan Meteorological Agency (JMA). The MRI-EPS has the ability to calculate initial perturbations in the southern hemisphere (SH) as well as in the northern hemisphere (NH) and tropical region (TR). The perturbations used for ensemble forecasting are made with a breeding of growing mode (BGM) methodology.

This report outlines the MRI-EPS and explains the fundamentals relevant to ensemble prediction. The MRI-EPS can generate initial perturbations separately for the NH, SH, and TR. For convenience of users, daily perturbations of the NH and the SH up to 25 modes and perturbations of the TR up to two modes have already been calculated and stored for the period from 1 October 2001 to 31 March 2013. The MRI-EPS is therefore ready to perform ensemble prediction experiments using these perturbations for the global region with a lead time up to 34 days. A detailed Japanese manual for users of the MRI-EPS at MRI is also provided as an Appendix of this report.

To evaluate the performance of the MRI-EPS, we conducted the following two forecast experiments: we assessed the influence of the newly obtained SH perturbations on the forecast skill for the SH; and we investigated the predictability of the stratospheric sudden warming (SSW) that occurred in December 2001, an event that was thoroughly examined by Mukougawa *et al.* (2005). As a result, we found that the SH perturbation improves the forecast skill for the SH as well as the NH perturbation does for the NH. We also found that the skill of prediction of the December 2001 SSW was almost the same for the MRI-EPS and the JMA operational system. Furthermore, we found that application of the perturbations obtained with the MRI-EPS were very useful to predictability studies using the MRI climate model.

要旨

気象研究所における気候研究の促進を目的に、新しいアンサンブル予測システムを開発した。新しいシステム（MRI-EPS (BGM)：BGM 法に基づく気象研究所アンサンブル予測システム）は、気象庁の現業 1 か月予報用に開発されたアンサンブル予報システムを元にして北半球や熱帯域のみならず南半球の摂動まで計算できるよう拡張することによって構築した。アンサンブル予測に用いる摂動は、成長モード育成法（BGM 法）によって作成される。

本報告では、MRI-EPS の概要を記述し、また、アンサンブル予測手法に関する基礎的事項について説明する。MRI-EPS では、北半球、南半球、および熱帯の各領域における摂動を個別に計算することができる。北半球および南半球の各 25 摂動モードと熱帯の 2 摂動モードについては､既に 2001 年 10 月 1 日から 2013 年 3 月 31 日までの計算を完了している。従って、これらの期間については計算済摂動を用いた、最大 34 日積分のアンサンブル予測実験を直ちに行うことが可能になっている。本報告の付録では、気象研究所ユーザーに対する、詳細な MRI-EPS の日本語利用マニュアルも掲載した。

MRI-EPS の性能を評価するために、次の二種類の予報実験を行った。一つは、新しく計算可能とした南半球摂動を用いて、南半球の予報成績に対する効果を調べるもので、もう一つは、向川ほか(2005)でも調査された、2001 年 12 月の成層圏突然昇温に対する予測可能性に関する調査である。その結果、南半球摂動は、北半球に対する北半球摂動と同様に、南半球の予報精度の改善に貢献することが確かめられ、また、MRI-EPS による 2001 年 12 月の成層圏突然昇温の予測可能性は、当時の気象庁現業システムによるものと概ね同様であることが確認できた。さらに MRI-EPS によって得られた摂動は、気象研究所の気候モデルを用いて予測研究に適用する際に非常に有用であることが分かった。

Contents

1. Introduction

Numerical weather prediction (NWP) models as well as climate prediction models are constructed on the basis of deterministic governing equations that describe dynamical and physical processes that take place in the real atmosphere. Because the strong nonlinearity that exists in the governing equations produces chaotic motions, Lorenz (1963) remarked that numerical prediction of atmospheric motions eventually loses its skill after a certain forecasting period because of the inevitable growth of initial observational errors. Such non-deterministic behavior is the most important characteristic of chaotic motion. The inability of a NWP model to represent real atmospheric motions perfectly also reduces the predictive skill of numerical weather forecasts. In fact, the predictable period for synoptic-scale disturbances, such as mid-latitude low-pressure systems, is limited to several days, even in a state-of-the-art NWP system, and it is very hard to extend the predictable limit longer than two weeks with a deterministic prediction starting from a single initial condition.

Use of an ensemble prediction has been proposed as a way to extend the predictable limit of two weeks associated with deterministic prediction. The tactics of an ensemble prediction can be summarized as follows: generate slightly different initial conditions, the variability of which reflects the estimated observational errors; perform a model integration for each ensemble member, starting from the corresponding initial condition; and construct ensemble statistics from the predictions of all members. These statistics can provide valuable additional information for the prediction of atmospheric motions. The first statistic of the ensemble prediction is the ensemble mean, which characterizes the average scenario of the prediction. The second statistic is the ensemble spread, which indicates the uncertainty of the prediction and is a measure of the chaotic behavior of atmospheric motions. Finally, the probability distribution function (PDF) of the predicted variables, constructed from all ensemble members, sometimes provides further information: if the PDF has a bimodal distribution, for example, the ensemble prediction implies the possibility of dual prediction scenarios.

In an ensemble prediction, the most important issue is how to generate slightly different perturbations at the initial time. Although an infinite number of initial perturbations would be needed for the ensemble prediction to fully represent the distribution of an initial observational error, for practical reasons the ensemble size is limited to on the order of 100 because of computational resource limitations. Since the 1980's, NWP centers around the world, including the Japan Meteorological Agency (JMA), have started addressing a technical problem: establishing an operational long-range forecasting system by development of a practical ensemble prediction method that represents the distribution of observational errors with an affordable number of initial

perturbations.

During an earlier period of development, an attempt was made to use a Monte Carlo method to add randomly generated perturbations to the analysis field. However, this attempt was found to be in vain because most of these perturbations have large projections on gravity wave modes, and the contribution to modes related to synoptic eddies is very limited. Thus, an infeasibly large number of initial perturbations would be required for the Monte Carlo method to obtain an appropriate ensemble spread.

Another convenient ensemble forecasting method is the so-called LAF (lagged average forecast) method. In this method, the ensemble is composed of deterministic forecasts that start at different initial times. Here, the addition of perturbations to the initialized fields is not required, and a single model run from each initial time suffices for constructing a LAF ensemble. However, a concern with the LAF method is that ensemble members that start from earlier initial times always degrade the quality of the prediction. This issue is crucial for a prediction with a lead time shorter than a few weeks, because the interval of the neighboring initial times is not so short (commonly 6 hours); the interval is determined by the period of the operational global analysis cycle of NWP centers. Moreover, it is not assured that the observational error field at the initial time is suitably represented by the forecasts of LAF ensemble members starting from earlier initial times.

To efficiently represent the initial observational error with a finite number of initial perturbations, the following two approaches for generating initial perturbations based on dynamical considerations have been suggested in recent years: the singular vectors (SV) method and the breeding of growing mode (BGM) method. For these methods, it is expected that the initial spread among ensemble prediction members will be large enough to represent observational errors. The SV method and the BGM method were designed and have been used for operational extended-range (up to about two weeks) forecasts since 1992 by the European Center for Medium-Range Forecasts (ECMWF) and the National Meteorological Center in the United States (NMC, now known as National Centers for Environmental Prediction: NCEP), respectively.

In the SV method, initial perturbations are composed of the fastest-growing modes over a specified short time interval (which is typically shorter than 48 hours) based on a tangent linear model, which is obtained by locally linearizing the original nonlinear NWP model, and its adjoint model (e.g., Buizza *et al*., 1993). The modes are obtained by singular value decomposition (SVD) of the so-called error matrix describing the linear evolution of initial perturbations over the specified time interval. The associated singular value gives the rate of linear amplification of the singular vector over the specified period.

In the SV method, it should be noted that the initial perturbation specified by the singular vector does not necessarily show the largest growth in the original NWP model during a time interval of several days because of the emergence of nonlinearity of the initial perturbation during its

growth. Moreover, because the original NWP model has a huge number of degrees of freedom and includes various dynamical and physical processes that interact with each other, it requires several practical compromises in using the tangent linear model: omission of several physical processes in the model; selection of a limited number of variables to construct the error matrix; and use of a large-scale model that neglects motions on a scale smaller than synoptic eddies by truncating the spatial resolution of the original NWP model, thereby reducing the size of the error matrix.

In spite of these practical issues, the SV method brought about a remarkable improvement compared to the LAF method with respect to the spread-skill relationship, in which a larger ensemble spread corresponds to an ensemble mean forecast with less skill. The SV method has thus been recognized as one of the most promising ensemble techniques for medium-range ensemble forecasts. Today, the SV method is used in medium-range ensemble forecasts at the ECMWF and the JMA, and also in ensemble typhoon forecasts and meso-scale severe weather forecasts (e.g., Yamaguchi *et al*., 2009).

In the BGM method, the perturbations used to construct the ensemble members are given by so-called bred vectors, which are disturbances obtained by integrating the NWP model from small arbitrary initial perturbations over a long time interval before the initial time of forecast. In the course of the long integration, perturbations are rescaled over short cycles, called BGM cycles, whose interval is typically 12 hours, and integrated again. At the end of the BGM cycles, all perturbations are scaled to a desirable amplitude. These scaled perturbations make up the initial perturbations for the ensemble forecasts (Toth and Kalney, 1993; Legras and Vautard, 1995). More specifically, in each BGM cycle, integration of the NWP model over a short period of time is performed from an initial condition consisting of the superposition of a perturbation onto the analysis field (perturbed run). A mature perturbation is then obtained by subtracting the analysis field from the forecast of the perturbed run at the end of the BGM cycle. The magnitude of the mature perturbation is evaluated with respect to a given norm, such as an area-averaged variance at a geopotential height of 500 hPa over a specified region, or the total energy norm of the perturbation. The mature perturbation is rescaled to a specified magnitude based on the norm and is used as the initial perturbation for the next BGM cycle. After many BGM cycles over a long enough time interval, an optimal initial perturbation is obtained. The optimal initial perturbation is called a bred mode; it is the perturbation with the largest growth rate over the previous time interval. The bred modes correspond to the local Lyapunov vectors when a perfect model assumption is adopted by replacing the analysis with the forecast (control run), starting from the initial condition without any perturbation at the end of each BGM cycle. The tangent linear model is used there to evaluate the evolution of the perturbation over time.

Compared with SV methods, the BGM method has the advantage of using the original nonlinear NWP model to evaluate the evolution of perturbations over time. However, the BGM

method has an additional computational cost associated with the multiple BGM cycles required to generate the initial perturbations for conducting the ensemble forecast. The NCEP has confirmed that the BGM method has the ability to improve the forecast skill of medium-range predictions (Toth and Kalney, 1997). The NECP and JMA now use the BGM method operationally for medium-range and seasonal ensemble forecasts.

The JMA uses the BGM method for operational one-month and seasonal ensemble forecasts and uses the SV method for operational one-week and typhoon ensemble forecasts.

We have recently constructed a new global atmospheric ensemble forecasting system that uses the BGM method [MRI-EPS (BGM)] on the supercomputing system of the MRI. The MRI-EPS facilitates MRI research activities concerned with climate variation and the predictability of atmospheric motions by conducting medium range or sub-seasonal range ensemble forecast experiments. This report provides an outline of the MRI-EPS, directions for how to use the system, and a description of the characteristics of the bred vectors obtained with the MRI-EPS. This article also presents results of ensemble forecast experiments conducted with the MRI-EPS for the prediction of a stratospheric sudden warming (SSW) event.

2. Outline of the MRI-EPS

The MRI-EPS includes BGM cycle system running on the MRI supercomputer system, which is developed by using the operational one-month forecasting system by the Climate Prediction Division (CPD) of the JMA (Kyoda, 2000, 2006), hereafter referred to as the JMA-BGM, as reference. Although the basic specifications of the BGM cycle in the MRI-EPS and JMA-BGM are almost the same, the MRI-EPS is able to generate perturbations in the southern hemisphere (SH), which is not represented in the JMA-BGM. This capability facilitates predictability studies for SH atmospheric motions, such as the SH SSW that occurred in 2002. The following is an outline of the MRI-EPS.

2.1 NH BGM cycle

Figure 1 illustrates the BGM cycle of the MRI-EPS for the northern hemisphere (north of 20°N, hereafter referred to as NH). The cycle time interval is 12 hours, and the adopted norm of the perturbation is the area-averaged variance of the 500-hPa height (Z500) in the NH. At the start of the BGM cycle (00 or 12 UTC), two different initial fields are prepared: one is the control initial condition provided by the analysis field (black circle in Figure 1), and the other is a perturbed initial condition produced by the superposition of a perturbation on the analysis field (colored circle). Then the NWP model is integrated for 12 hours, starting from both initial conditions. These runs are called the control run and perturbed run; they are indicated by the black and blue arrows, respectively, in Figure 1. The difference field *D* between the two forecasts after 12 hours (denoted by the thick dotted arrows) is regarded as a mature perturbation over the course of the BGM cycle. When the perturbation is determined by the difference of the perturbation run, but not from the

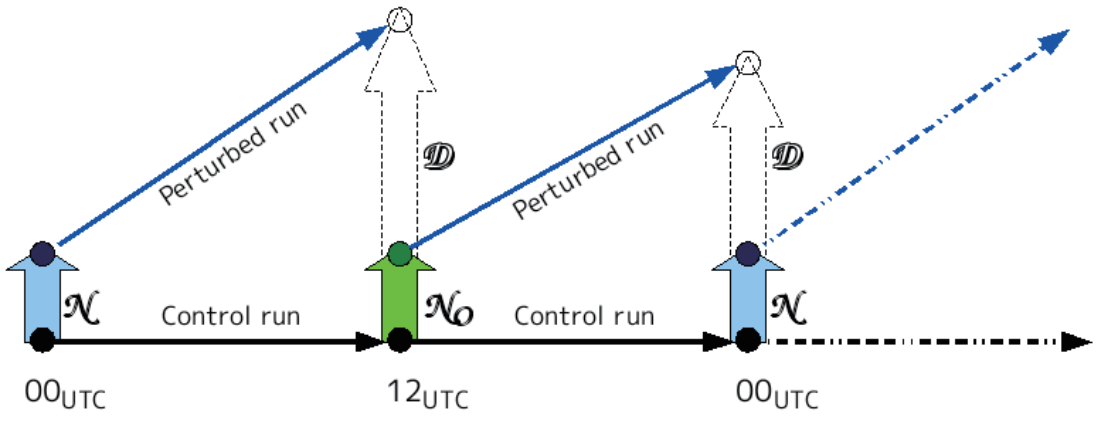

Figure 1: Conceptual diagram of the BGM cycle in the MRI-EPS.

analysis, such a BGM method is called a self-breeding. This type of BGM cycle is adopted in the MRI-EPS and has the desirable characteristic of removing the influence of model bias, which is included in both the perturbed and control runs, on the evaluation of the instability mode of the model.

The difference field D is normalized ("scaled down") so that the norm of D_{Z500} (Z500 difference field) becomes specified value and is subsequently used for an initial perturbation in the next BGM cycle (the normalized perturbation, denoted as N, is shown by the thick colored arrows in Figure 1). Here, the rescaling is carried out so that the area-averaged variance of D_{Z500} in the NH has a magnitude equal to 14.5% of the climatological variance of Z500, which depends on the seasonal cycle. Although the norm is evaluated by the Z500 field, there is rescaling of other forecast variables, such as the height field, horizontal winds, temperature, specific humidity at 23 pressure levels, and surface pressure. The perturbation is normalized by multiplying by the same rescaling factor used to rescale the Z500 field[1]. Furthermore, in the region south of 20°N, the magnitude of the normalized perturbation N is reduced exponentially as follows:

$$N(\varphi) = N_{ext}(\varphi) \exp(- (\varphi - 20)^2/50) \qquad (1)$$

where φ is the latitude in degrees and $N_{ext}(\varphi)$ is a normalized perturbation in the extra-NH region ($-90 < \varphi < 20$). The perturbed run in the next BGM cycle then starts from an initial condition consisting of the perturbation N, tapered in the extra-NH region by Eq. (1), and the analysis field.

In the MRI-EPS, the initial NH perturbation is obtained every 12 hours with the foregoing BGM cycle. To obtain several initial perturbations to carry out ensemble forecasts with multiple members, similar BGM cycles that start from several initial perturbed fields are conducted simultaneously. In the MRI-EPS, normalized perturbations are (quasi-)orthogonalized with each other at 12UTC by using a method similar to Gram-Schmidt[2], in accord with the JMA-BGM. The obtained orthonormalized perturbations *No* are shown by thick green arrows in Figure 1. Obtained modes are numbered according to the order of the BGM cycle series. That is, the first mode (also referred to as mode #1) corresponds to the first BGM cycle series and is free from the orthogonalization. In contrast, perturbation of mode #n ($n \geqq 2$) is derived from the n-th BGM cycle series and is orthogonal to perturbations of mode #1, #2, . . . , and #n–1.

To obtain a converged bred mode at the initial time of forecast, we have to conduct a very large number of BGM cycles prior to the initial time. The MRI-EPS aims at rapid convergence of the

[1] In the stratosphere (above 100 hPa height), the factor is multiplied by p/100 at pressure p [hPa] to reduce the amplitude of the perturbation. Otherwise, the stratospheric perturbation has a much larger amplitude compared to the estimated analysis error.

[2] A quasi-orthogonal vector y, obtained from the vector x, to the other vectors $\{x_i\}$ is expressed by $y = x - a \Sigma_i < x_i , x > x_i$, where a is called the orthogonalization ratio ($0 < a < 1$, set to 0.75 in the MRI-BGM).

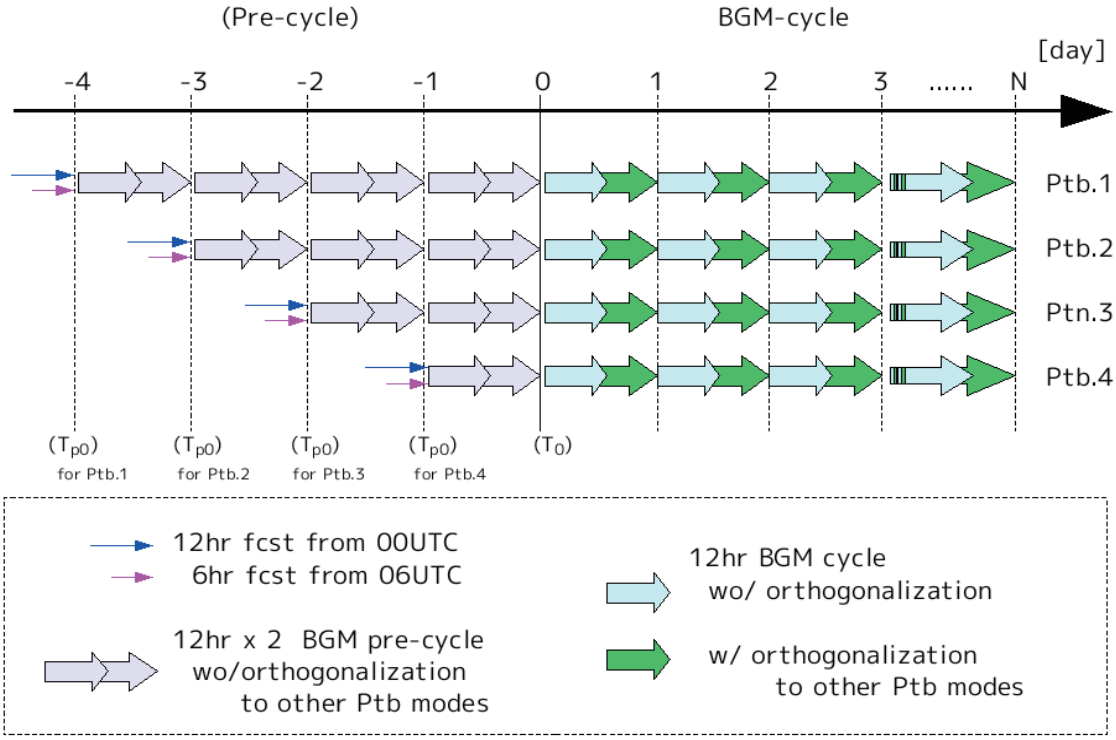

Figure 2: Flow image of pre-cycle and the following BGM cycle

bred vector, and a simple additional pre-cycle is devised by using the concept of the LAF method, as shown in Figure 2. For example, the initial perturbation necessary to initiate a pre-cycle starting from 12 UTC in one day (denoted by T_{p0} in Figure 2) is given by the difference field obtained from the following two control runs without initial perturbations: one control run starts at an initial time 6 hours prior to T_{p0} (i.e., 06 UTC); the other starts 12 hours prior to T_{p0} (i.e., 00 UTC). These two runs are denoted by purple and blue arrows, respectively, in Figure 2. The normalized difference field between the two runs at T_{p0} is then regarded as the first perturbation for the pre-cycle. We subsequently repeat the pre-cycle, including the rescaling procedure every 12 hours, as in the BGM cycle, until the starting time of the BGM cycle (T_0), shown by thick gray arrows in Figure 2.

To obtain several initial perturbations, we have to proceed through several series of pre-cycles, starting every 12 UTC several days prior to T_0. For instance, if we need four perturbations, we proceed through four different series of pre-cycles, starting from 12 UTC on each of the four days prior to T_0. In the pre-cycle, orthogonalization of perturbations is not conducted. Thus, the perturbations obtained from each pre-cycle series are independent of each other. After obtaining the required number of perturbations with the pre-cycles, the main BGM cycle (denoted by the light and dark green arrows in Figure 2) starts at time T_0. From our experience, perturbations generated in the BGM cycle of the MRI-EPS, after the above-mentioned pre-cycles have been conducted, acquire a well-defined spatial structure, similar to synoptic-scale disturbances over a bred

cycle of several weeks. We can therefore use the MRI-EPS to proceed with subsequent ensemble prediction experiments.

2.2 Tropical BGM cycle

In the extra-tropical atmosphere, the perturbations that grow and become dominant are related to the baroclinic instability of westerly jets in the troposphere. Such unstable baroclinic modes are basically characterized by geostrophic modes, the temporal evolution of which is well represented by geopotential height variations in the troposphere. Hence, we have used the area-averaged variance of Z500 to define the norm used to evaluate the amplitude of growing perturbations in the NH BGM cycle. In contrast, in the tropical region, atmospheric modes with divergent motions dominate over geostrophic modes (Rossby mode). Hence, another type of norm should be used to generate growing perturbations appropriate for ensemble predictions of the tropical atmosphere. According to Chikamoto *et al*. (2007), an area-averaged variance of the 200 hPa velocity potential (hereafter χ200) over the tropics from 20°S to 20°N is appropriate for the norm of the perturbations of the BGM cycle in the tropics (TR BGM cycle). Moreover, the normalized perturbation during such a tropical BGM cycle is exponentially damped poleward in the extra-tropics, as is the case for the NH perturbation described by Eq. (1).

According to Chikamoto *et al.* (2007), the time interval of each TR BGM cycle is set to 24 hours to extract slowly growing, large-scale modes of the tropical atmosphere (whereas the time interval of the NH BGM cycle is 12 hours). Both normalization and orthogonalization of the mature perturbation are done at the end of every TR BGM cycle. The rescaling factor is specified, as in the TR BGM cycle of the JMA-BGM system, such that the norm of the perturbation becomes 20% of the climatological variance of χ200.

We have confirmed that initial perturbations in the tropics obtained by these parameter settings of the TR BGM cycle grow continuously over a forecast period of more than five days in the MRI-EPS forecast experiments. We therefore think that the obtained tropical bred modes are suitable for use as initial perturbations in ensemble forecast experiments for the tropical atmosphere.

The developed TR BGM cycle in the MRI-EPS does not include a pre-cycle like the pre-cycle used in the NH BGM cycle; instead, it starts from initial perturbations given by the previously obtained NH bred modes[3]. Although the amplitude of the NH bred mode is rather small in the tropical region because of the artificial damping by Eq. (1), we have confirmed that these tapered perturbations also grow with an e-folding time of about 10 days. Hence, the computed tropical bred modes have converged enough over BGM cycles of several weeks to comprise the initial perturbation for the ensemble forecast experiment in the tropical atmosphere. There are only two tropical bred modes available in the MRI-EPS because the higher bred modes in the tropics have

[3] Or by TR bred modes previously calculated by another TR BGM cycle experiment, if they exist.

spatio-temporal characteristics similar to these two bred modes.

2.3 SH BGM cycle

One of the important merits of the newly developed MRI-EPS is the inclusion of initial perturbations in the southern hemisphere (SH); such perturbations are not used in the operational monthly and seasonal EPSs of the JMA. The exclusion of SH perturbations in these JMA operational EPSs is, of course, due to the practical consideration that the primary target region for the JMA weather forecasts is the NH, including Japan, but not the SH. However, in order to conduct ensemble forecast experiments for the global atmosphere (including the SH atmosphere), we have to prepare initial perturbations in the SH. In particular, these perturbations are indispensable for exploring the predictability of the predominant atmospheric motions in the SH, such as the SH SSW and the southern annular mode (SAM).

The MRI-EPS system is capable of simulating a SH BGM cycle, a BGM cycle for the SH (south of 20°S). The parameter values and procedures, such as the norm, time interval of each cycle, and the rescaling and orthogonalization method are determined in the way described in Section 2.1 for both the SH and NH BGM cycles. We discuss the effects of the newly obtained SH bred modes on the forecast skill of the ensemble predictions for the SH atmosphere in Chapter 4.

2.4 Forecast model and ensemble forecast experiments

The atmospheric forecast model used in the MRI-EPS is the JMA atmospheric global spectral model (GSM), which has been used in the operational one-month ensemble forecast system as of March 2013. This is a global hydrostatic spectral primitive model with a TL159 reduced Gaussian horizontal grid; the grid size is about 120 km around the equator and becomes coarser toward the poles. The model includes 60 vertical layers arranged up to 0.1 hPa based on the η (σ-p hybrid) coordinate system. A two-time-level, semi-Lagrangian integration scheme has been adopted to carry out the integration over time efficiently.

The model includes several schemes that parameterize processes representing radiative interactions with atmospheric molecules, clouds and aerosol particles, cloud schemes that predict cloud water content and diagnose cloud amount, a mass-flux type cumulus convection scheme, and a planetary boundary layer scheme that evaluates turbulence in the lower tropospheric near the surface. Heat and hydrological balances associated with these processes are calculated every time step during integration of the model (note that the radiation scheme is run every several time steps). Moreover, the model includes processes that generate and break orographic gravity waves, which are not explicitly resolved in the model. To specify the surface boundary condition of the atmospheric model, a SiB type land surface scheme is also included in the model. Observed sea surface temperature (SST) anomalies at the initial time are kept constant over the forecast period; they are added with the

climatological SST to specify the surface boundary conditions over the sea. The climatological sea-ice distribution is specified during the forecast period. Refer to the JMA web page[4] for details of the atmospheric and land surface model.

Ensemble forecast experiments with the MRI-EPS are performed using the global atmospheric model described above, with initial perturbations generated by the BGM cycle system of the MRI-EPS according to the following procedure. First, the initial conditions for forecast experiments are specified by obtaining initial perturbations as well as analysis (or climatological) data for the atmosphere, land, and sea surface. The initial time of the model integration is set to 12 UTC on a given day. The MRI-EPS can specify initial perturbations for each region of the NH, TR, and SH, as described in Chapter 2, and for the entire globe as well by using a combination of the three perturbations. For example, if the focus of interest is on the northern hemisphere, it is appropriate to combine the NH and TR perturbations without the SH perturbation (refer also to the last paragraph of Chapter 4). Perturbed initial conditions for the MRI-EPS are created by the analysis with addition (ensemble member is referred to as a name including the symbol "p") or subtraction (member name including the symbol "m") of perturbations generated with the BGM system. Hence, taking account of the control forecast without an initial perturbation, the ensemble size (number of members) of the MRI-EPS becomes 2N + 1, where N is the number of generated bred modes. Table 1 explains the naming rules for the ensemble members of the MRI-EPS. Since NH and SH perturbations are generated by using the same configuration of the BGM cycle system, these perturbations are named on the basis of the number of the bred mode with the symbols "p" or "m"; the names also specify the names of the ensemble members. In contrast, because there are only two generated TR modes, the first and the second TR bred modes are used to construct the initial perturbations for the even- and odd-numbered MRI-EPS ensemble members, respectively, in accord with the JMA operational EPS system.

Table 1: Rules for naming MRI-EPS ensemble members.

Member name	M00	M01p	M01m	M02p	M02m	M03p	M03m	M04p	M04m	.....
Ptb.mode (NH)	—	01p	01m	02p	02m	03p	03m	04p	04m	.....
Ptb.mode (TR)	—	01p	01m	02p	02m	01p	01m	02p	02m	.....
Ptb.mode (SH)	—	01p	01m	02p	02m	03p	03m	04p	04m	.....

[4] http://www.jma.go.jp/jma/jma-eng/jma-center/nwp/outline2013-nwp/pdf//outline2013_03.pdf (at the time of writing)

Second, the model integration is carried out starting from the initial conditions specified by the foregoing procedure. During the integration, the land surface conditions are predicted by the land surface model, the SST anomaly is kept constant, and the distribution of sea ice is specified by a daily climatology, as in the BGM cycle. When a standard setting of the MRI-EPS system has been chosen, forecast data such as altitude, temperature, and wind speeds are stored at six-hour intervals on latitude-longitude grids with a 1.25-degree spacing at the specified pressure levels, in a so-called pressure-level file.

3. How to execute ensemble forecast experiments with the MRI-EPS

In this chapter, we briefly describe a standard procedure for executing ensemble forecast experiments with the MRI-EPS on the MRI supercomputer system. Users of the MRI supercomputer system can also refer to the Appendix of this report, written in Japanese, in which a detailed description is provided of technical information such as execution commands and configuration files for the experiments.

3.1 Preparation of the computational configuration

Before initiation of the BGM cycle and/or an ensemble forecast experiment with the MRI-EPS, computation configurations are constructed by preparation of necessary files. After a compressed system file named MRIBGM.tar.gz has been obtained, copied to a specific directory, and uncompressed the file, the system directory (hereafter denoted by $BGMDIR) for the BGM cycle and the ensemble prediction is accessible. The directory contains shell script files to perform the experiments, execution files such as programs to compute the norm of bred modes, programs that describe the atmospheric model, and various utility program files mentioned in subsequent sections.

Next, analysis data must be prepared for the atmosphere and land conditions, SST, and distribution of sea-ice. These data are needed as input data for the experiments. It should be noted that these analysis datasets should be provided with the same data format as is used in the operational JMA system, namely NuSDaS format. The JRA-25 reanalysis data, land surface data from the JMA/CPD offline analysis, and COBE-SST sea-surface data (see also Table 2) during the specified experimental period (including the period for the pre-BGM cycle) should be stored in some directories of the supercomputing system of the MRI before starting the experiments. It should be noted that in this version of the MRI-EPS the land surface data are given by the climatology and are rearranged on reduced-Gaussian grid points the grid spacing of which depends on the specification of the atmospheric model.

Table 2: Analytical data used in the experimental system

	dataset name	time interval	spatial resolution	refference
Atmosphere	JRA-25 reanalysis	6 hourly	1.25x1.25 degs 23 p-levels	Onogi et al. (2007)
Land	JMA/CPD offline analysis	12 hourly	TL159 reduced-gaussian grid	JMA/CPD (Tokuhiro)
Sea surface	COBE-SST dataset	daily (18UTC)	1 x 1 degs	Ishii et al. (2005)

3.2 Execution of the NH BGM cycle

If there is no previously obtained bred mode, the pre-cycle must be executed first. In that case, a shell script file named pre_nh*p.sh in $BGMDIR (* corresponds to 4 or 25) is properly edited and executed. Adequate computational configurations for the pre-cycle for 4 or 25 bred modes on the MRI system should then exist. Each pre-cycle for a NH perturbation can then be started. A flow chart for each pre-cycle is shown in Figure 3. Here, “Bg” stands for a 12-h or 6-h forecast job. For example, Bg1200 means a control run starting from 12 UTC, whereas Bg0001p is a perturbed run (mode number 01) starting from 00 UTC. “Stan” job rescales the mature perturbation after evaluating its norm at 00 UTC and 12 UTC. “Cpcycl” job saves the generated perturbation in the pre-cycle and prepares for the transition to the next pre-cycle. The part denoted by “llsub_bgm_nh1p” in Figure 3 obtains the first perturbation of the pre-cycle from the difference field between the 6-h (BG0600 job) and 12-h (Bg00pre job) forecast. In contrast, “llsub_bgm_nh1” constructs the main part of the pre-cycle for each bred mode.

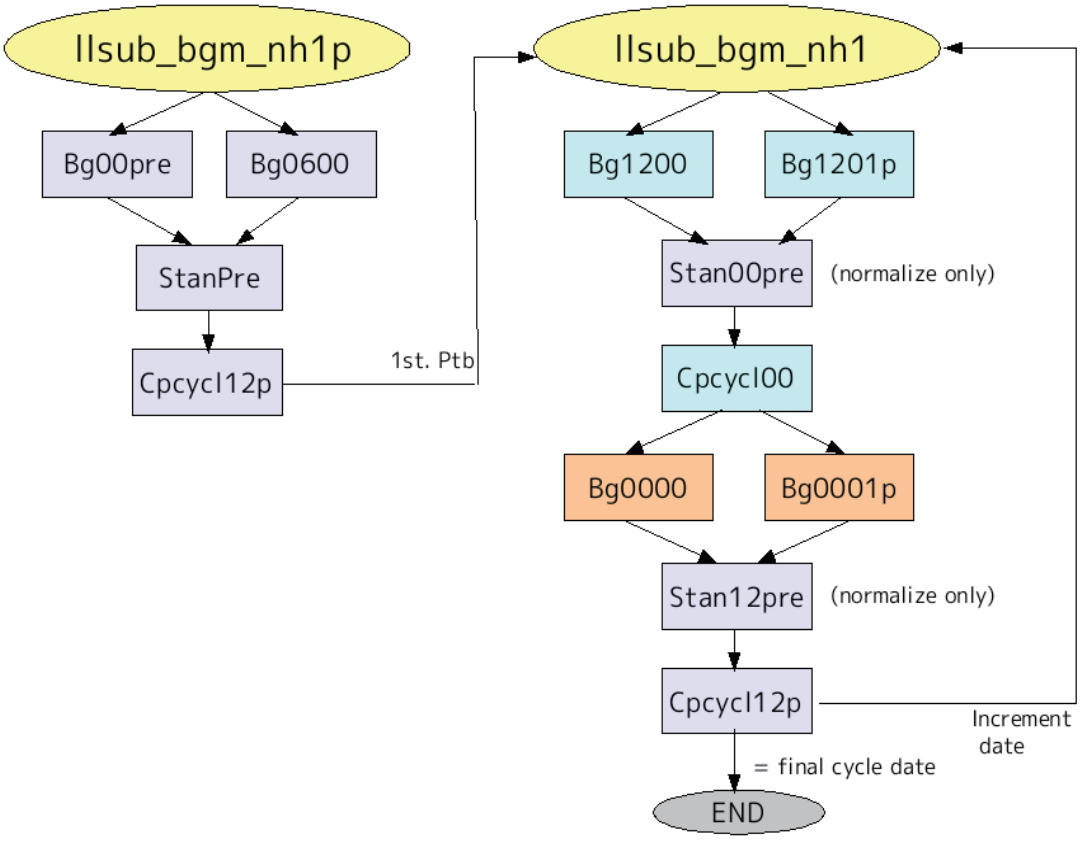

Figure 3: Flow chart of the pre-cycle for the NH perturbation

The main BGM cycle cannot be started until the initial perturbations have been obtained with the (4 or 25) series of pre-cycles. And it is ensured that there will be adequate computational configuration for the NH BGM cycle (to generate 4 or 25 bred modes) by proper edit and execution of a shell script file named $BGMDIR / pre_nh*.sh (* = 4 or 25). After those steps, the main BGM cycle can be started. Figure 4 illustrates a flow chart of the NH BGM cycle for four bred modes. In the main BGM cycle, the control forecast (Bg$$00) and four perturbed forecasts (Bg$$##p) can be carried out simultaneously if there are sufficient computer resources. Here, $$ indicates the initial UTC time (00 or 12), and ## indicates the bred mode number (from 01 to 04). The perturbations are only normalized at every 00 UTC by Stan00 job and orthonormalized to each other at every 12 UTC by Stan12 job. The obtained bred modes are stored in a directory specified in the shell script every 12 hours by Cpcycl jobs. At every 12 UTC, initial perturbations for the subsequent ensemble forecast experiment are created in addition to the perturbations needed to start the next BGM cycle. The former perturbations differ from the latter in the following two ways: (1) to retain the characteristics of each mode generated by the forecast model, there is no orthogonalization between perturbations; (2) the rescaled perturbations are multiplied by a weight factor to represent the global

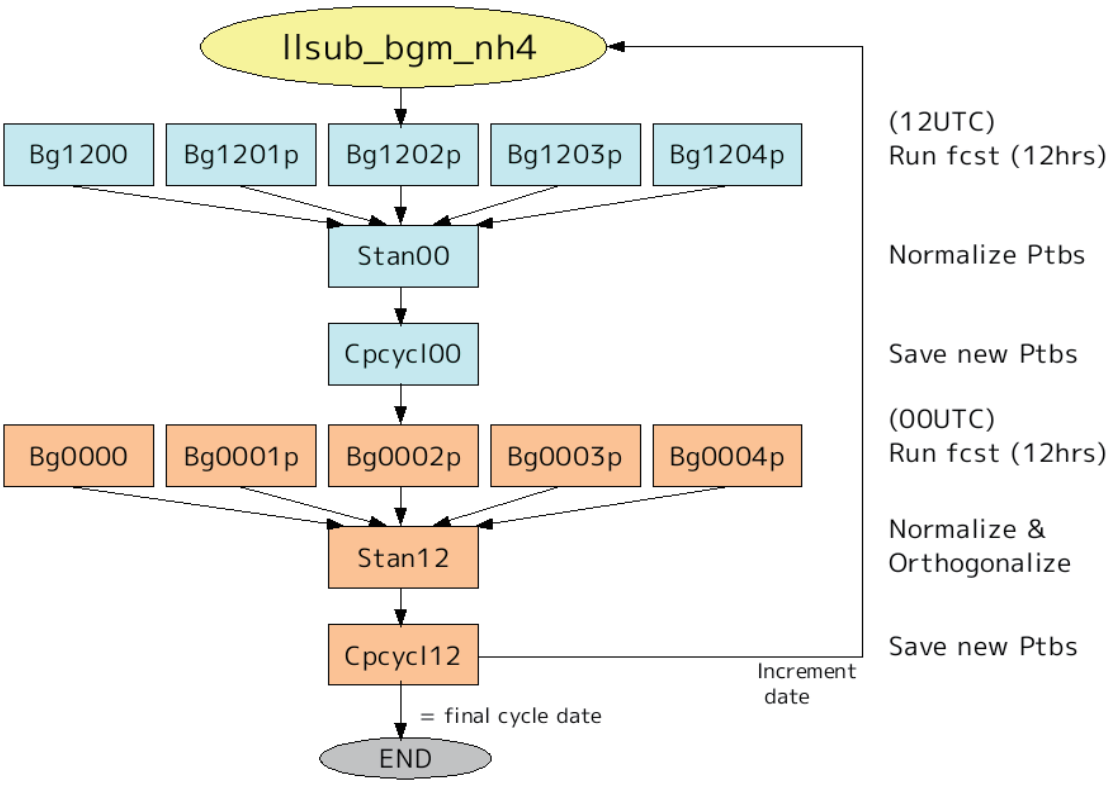

Figure 4: Flow chart of the NH BGM cycle (4-mode version)

distribution of analysis error in the atmosphere[5], because the reliability of the analysis data is not uniform on the globe.

When it is desired to extend a BGM cycle terminated normally or to restart a cycle unexpectedly terminated for a certain reason, it is necessary to replace the start date written in the shell script file with the first target date of the restart BGM cycle and to set the perturbation data directory so that it is identical to the perturbation directory used in the previous cycle. After those steps, the BGM cycle can be executed continuously.

3.3 Execution of the TR BGM cycle

If there is no proper initial perturbation to start the TR BGM cycle, the NH bred modes are used to start the cycle. A program located in the BGM Tool directory ($BGMDIR/Tool) is available to convert a NH bred mode into the initial perturbation needed to start the TR BGM cycle. The program will change only the metadata information about the region where the perturbation data are applied.

When the TR BGM cycle is started, a shell script file named $BGMDIR/pre_tro.sh must be properly edited and executed. Then there will be adequate computational configurations for the TR BGM cycle generating two TR bred modes. At that point, the main TR BGM cycle can be started on the supercomputer system of the MRI. Figure 5 illustrates a flow chart of the TR BGM cycle. It has basically the same structure as the NH BGM cycle shown in Figure 4. After control (Bgtr00) and

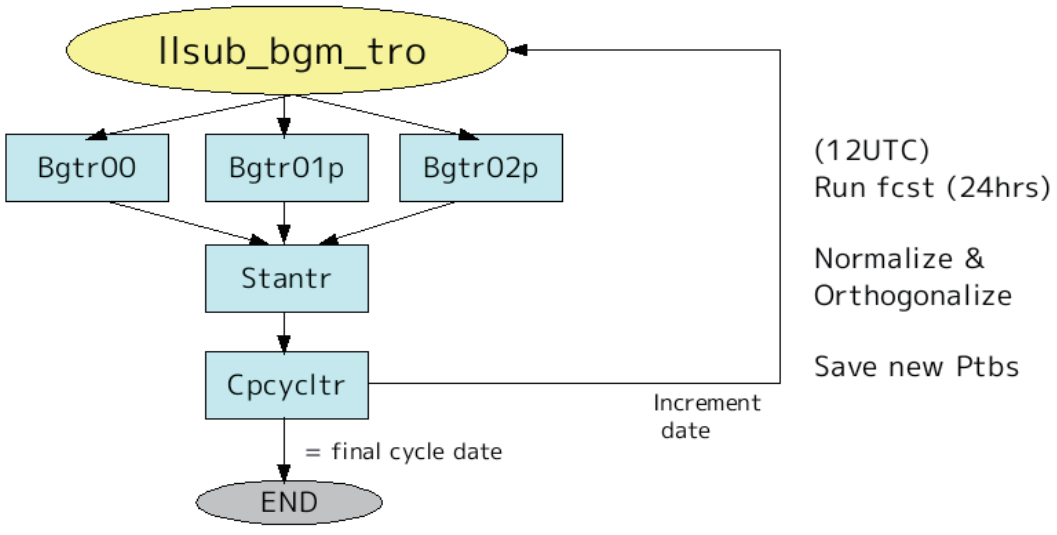

Figure 5: Flow chart of the TR BGM cycle

[5] MRI-EPS makes use of the same distribution of the weight factor for the analysis error (only in the NH) as is used in the JMA-BGM. See Kyoda (2000).

perturbed (Bgtr##p) forecasts for the prediction period of 24 hours (here, ## corresponds to a mode number) have been conducted, normalization and orthogonalization of the perturbations for the tropical region are carried out using a norm based on χ200 (Stantr). The orthonormalized perturbations are stored every 12 UTC in a specified directory (Cpcycltr) and are used to continue the TR BGM cycle. As is the case for the NH BGM cycle shown in Section 3.2, every 12 UTC another set of initial perturbations is also created, without conducting the orthogonalization process, for the following ensemble forecast experiment.

3.4 Execution of the SH BGM cycle

The SH BGM cycle to generate initial perturbations for the SH is performed in exactly the same manner as the NH BGM cycle: after a shell script file $BGMDIR/pre_sh*p.sh (* = 4 or 25: number of modes) has been properly edited and executed, there are adequate computational configurations for conducting the SH pre-BGM cycle and obtaining the initial perturbations for the main SH BGM cycle. The main SH BGM cycle is started by editing and executing a shell script file $BGMDIR/pre_sh*.sh (* = 4 or 25). Figure 4 is a flow chart of both the SH and NH BGM cycles. The obtained SH initial perturbations are stored every 12 hours in a specified directory.

3.5 Execution of the ensemble prediction experiment

The following is the procedure for conducting an ensemble forecast experiment by using the numerical atmospheric model (GSM) described in Section 2.4 from several perturbed initial conditions obtained with the BGM cycles described in Sections 3.2, 3.3, and 3.4. First, control and perturbed initial conditions must be established to start the forecast. After preparing the perturbation data and the analysis data (which have already been used in the BGM cycle), a shell script file $BGMDIR/make_lfin.sh must be properly edited, specifying preferable regions where initial perturbations are considered: a global perturbation for the NH, TR, and SH regions; a combination of perturbations for the NH+TR or SH+TR regions; and a perturbation for a single region (NH or SH). After the script has been executed, initial data from which numerical integrations of the GSM will be started are created for all ensemble members every day during a specified period.

To perform the forecast experiment, a shell script file $BGMDIR/pre_fcst.sh must be edited and executed. The control and perturbed runs are then executed by updating the initial date with an increment of 24 hours; the runs are carried out in parallel jobs if computing resources are available. Results of the forecasts describing predicted variables at specific pressure levels in the JMA NuSDaS data format are stored in a directory, specified in the script file, where results of each forecast member from each initial date are outputted in separate data directories.

4. Influence of SH bred vectors on the forecast skill for the SH atmosphere

In this chapter, we examine the effect of SH bred modes, which are newly obtained by the MRI-EPS system, to improve the forecast skill of medium-range prediction for the SH atmosphere. For this purpose, the BGM cycles of the MRI-EPS were executed to generate four bred modes for each of the NH and SH and two bred modes for the TR during February 2004. Two types of ensemble forecast experiments were then conducted with nine members (one control and eight perturbed members), both of which were started every 12 UTC during February 2004 with a prediction period of 30 days: one experiment (hereafter referred to as NTS) consisted of initial perturbations over the globe (NH+TR+SH region); the other experiment (hereafter referred to as NT) consisted of initial perturbations for the NH and TR regions, but not adding SH perturbations to the initial state.

Figure 6 shows the SH forecast score during the first week for the experiments started

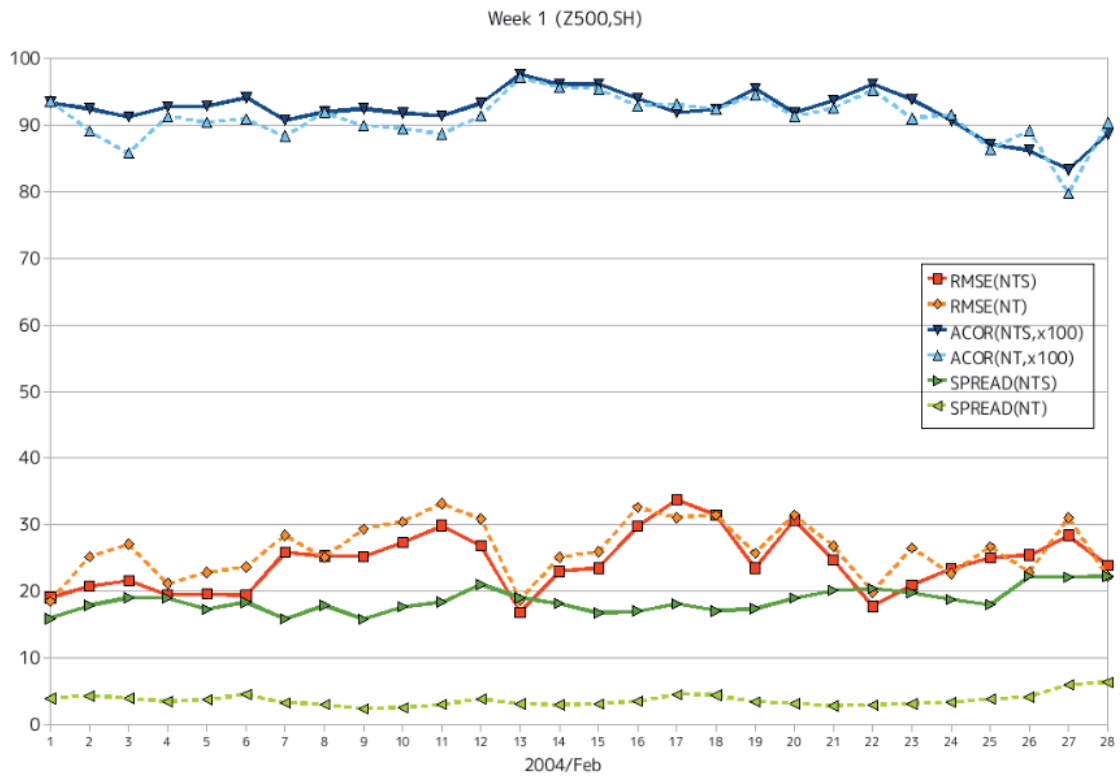

Figure 6: Scores of ensemble mean and ensemble spread (weekly mean Z500 in SH during the first week). Solid and dotted lines refer to the NTS and NT experiments, respectively. ACOR is multiplied by 100. The units of RMSE and SPREAD are meters. The horizontal axis shows the initial date of the ensemble forecast.

every day in February 2004. In this figure, RMSE and ACOR denote root mean square error and anomaly correlation coefficient, respectively, of the ensemble mean forecast for SH 500 hPa height. The magnitude of the ensemble spread is also shown by SPREAD in Figure 6. It is apparent that the ensemble spread is much larger for the NTS than for the NT. This difference reflects the fact that adequate SH initial perturbations were represented in the NTS, whereas very small-magnitude perturbations were added in the SH region of the NT. It is also apparent that the forecast skill of the ensemble mean prediction, assessed on the basis of the RMSE and the ACOR, is better for the NTS experiment than the NT experiment. Figure 6 also shows that the RMSE and SPREAD for the NTS are almost comparable in magnitude, but the SPREAD is slightly smaller than the RMSE.

Figure 7 shows the forecast scores for the second week. Although there are much larger variations among the forecasts compared to the first week, it is again apparent that the SPREAD of the NTS experiments, which is comparable in magnitude to the RMSE, is larger than the NT experiments. Figure 7 also indicates that, based on the RMSE and ACOR, the forecast skill in the SH for the NTS experiment, taking the SH perturbation into consideration, is improved overall compared with the NT experiment.

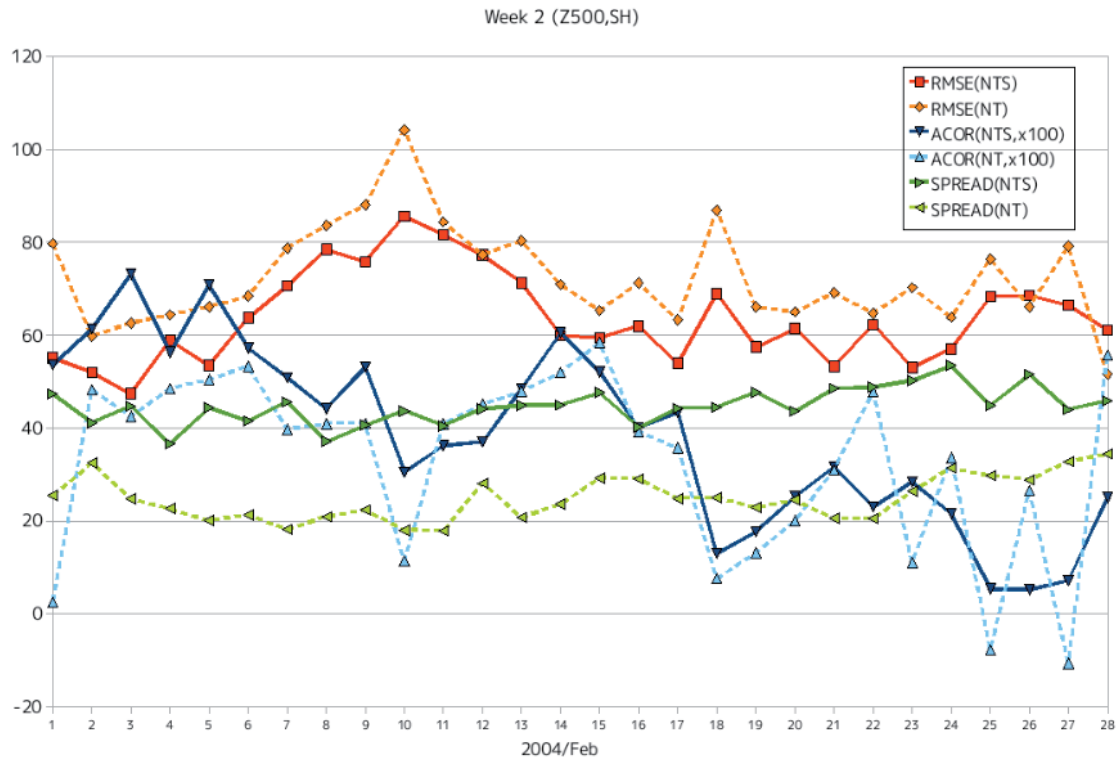

Figure 7: Same as Figure 6 except for the second week

Table 3 indicates the forecast skill and ensemble spread of the NTS and the NT experiments averaged over 28 forecasts, starting every day during February 2004. Here, W1 and W2 denote the mean value over the first and the second week, respectively. These data reconfirm that the forecast skill (RMSE and ACOR) is better and the ensemble spread (SPREAD) is larger for the NTS experiment than the NT experiment. Moreover, unlike the NT experiment, the average SPREAD for the NTS is similar in magnitude to the RMSE. The differences of the skill between the two experiments is statistically significant at the 99.9% confidence level, except for the ACOR in the second week.

From Table 3, it is also apparent that the SPREAD is smaller in magnitude than the RMSE, even for the NTS experiment. The small number of ensemble members (nine) may account for this difference. However, the rescaling factor for the SH BGM cycle, specified in the same way as for the NH cycle, may have been smaller than expected. If true, this would be another reason for the difference. Because the sparseness of observations in the SH lead to larger analytical errors compared to the NH, it is plausible that a larger rescaling factor should be specified for the SH. Moreover, consideration should be given to the fact that using an imperfect NWP model generally causes a smaller ensemble spread than using a perfect model (uncertainty of models, or parameterizations of the physical processes in the model, e.g. Buizza *et al*., 1999).

Finally, we also examined the forecast skill and ensemble spread of the weekly mean Z500 in the NH by using the same dataset of ensemble forecast experiments (i.e., NTS and NT). However, we found that there was no significant improvement in the NH score, although the SH perturbations were included in the NTS (not shown here).

Table 3: Forecast skill of ensemble mean forecast and ensemble spread.
(ACOR is multiplied by 100. The units of the RMSE and SPREAD are meters.)

Ptb. type	RMSE (W1)	ACOR (W1)	SPREAD (W1)	RMSE (W2)	ACOR (W2)	SPREAD (W2)
NTS	24.37	92.31	18.59	63.72	38.31	44.74
NT	26.30	91.09	3.63	72.40	33.10	24.92

5. Characteristics of a BGM perturbation

In this section, we examine the characteristics of the perturbation of the MRI-EPS created through the newly developed BGM system described in the previous sections. We also use the MRI-EPS to examine the predictability of the stratospheric sudden warming (SSW) that occurred in the winter of 2001 and compare the results with those obtained with the operational JMA-EPS.

By using the BGM system, we have already calculated and stored NH and SH perturbations up to 25 modes and TR perturbations up to 2 modes from October 2001 to March 2013. These perturbations can be used to immediately start ensemble forecast experiments. In this section, we show the result of an ensemble forecast experiment with the six leading NH bred modes. These bred modes were used to generate 13 initial perturbations by taking into account the polarities of six bred modes and the unperturbed control forecast. This configuration of the ensemble forecast is the same as the configuration of the operational JMA 1-month ensemble forecast for the winter of 2001. We conducted ensemble forecasts starting every day during the period from 28 November through 20 December of 2001, during which a SSW event was observed.

5.1 Spatial structure of bred mode

First, we examine the spatial structure of the obtained NH bred mode. Figure 8 shows a latitude-height cross section of the zonal-mean amplitude of the bred modes averaged over the 23-day experimental period. A common meridional distribution of the amplitude is apparent in the six bred vectors. In fact, the amplitude has two peaks: one is around 300 hPa at 40–50°N, and the other is around 300 hPa at 80°N. The peak at 40–50°N corresponds well with the latitude of the maximum amplitude of climatological synoptic waves (not shown) and also with the region of the maximum baroclinicity of the climatological zonal mean flow.

Figure 9 shows the horizontal structures of the 500-hPa geopotential heights for obtained bred modes on 13 December 2001; all ensemble forecasts starting from this date succeeded in forecasting the occurrence of the SSW (see Section 7.1). On this date, a very prominent blocking high was observed over England (not shown). Associated with this blocking, most bred modes had large perturbation amplitudes around the polar region. These large-amplitude perturbations correspond to the dominant peaks in the amplitudes of the bred modes shown in Figure 8. The observed flow might be highly unstable with respect to the bred mode, because the bred mode will grow due to the dynamical instability of the observed flow.

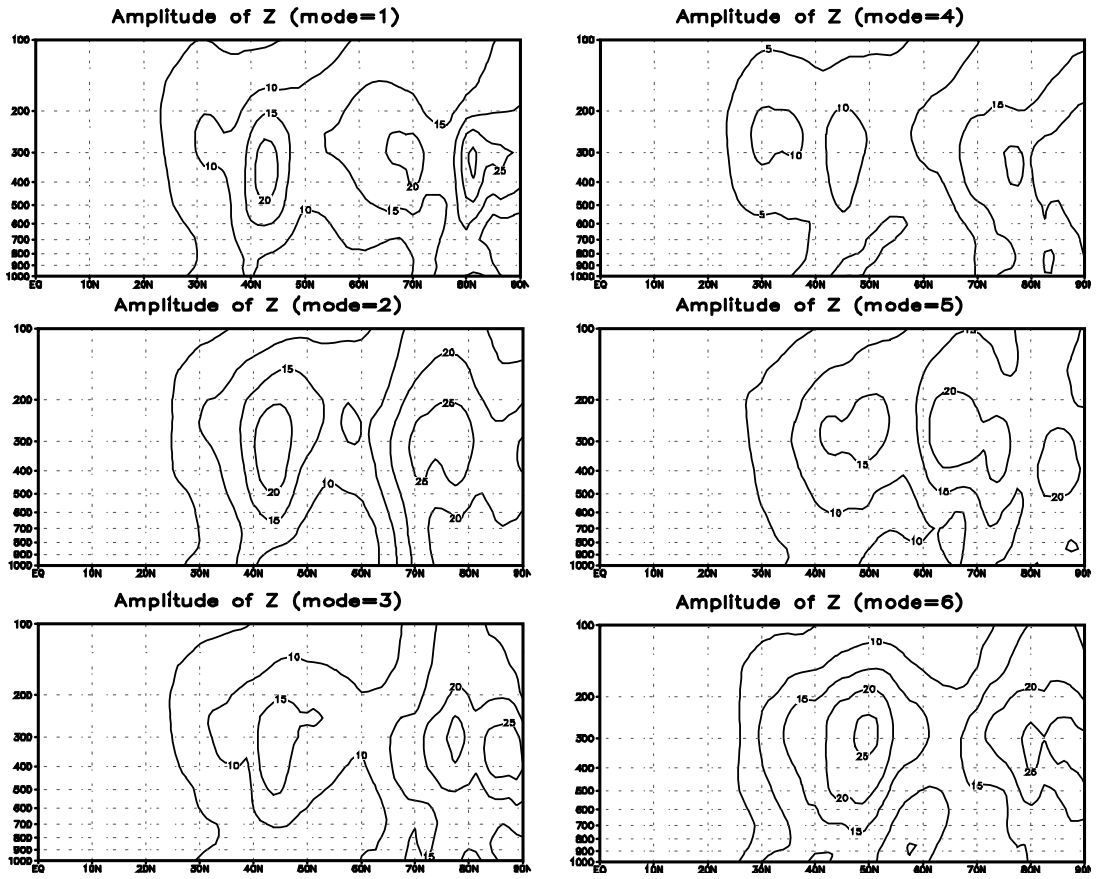

Figure 8: Zonally averaged amplitude of the geopotential height associated with the obtained bred modes. The amplitude was averaged over a period of 23 days from 28 Nov. to 20 Dec. 2001. Contour interval is 5 m.

We also examined the zonal wavenumber spectrum of the geopotential height amplitude of the bred mode. Figure 10 shows the geopotential height amplitude of the bred mode at 300 hPa averaged over 40–50°N as a function of zonal wavenumber. The spectrum was obtained from the average over 23 days of the experimental period. It is apparent that all bred modes have a peak around zonal wavenumber 5 and 6, except for the third mode, in which the highest peak in the spectrum occurs at zonal wavenumber 3. This result also suggests that the obtained bred modes grow through the baroclinic instability of the observed flow.

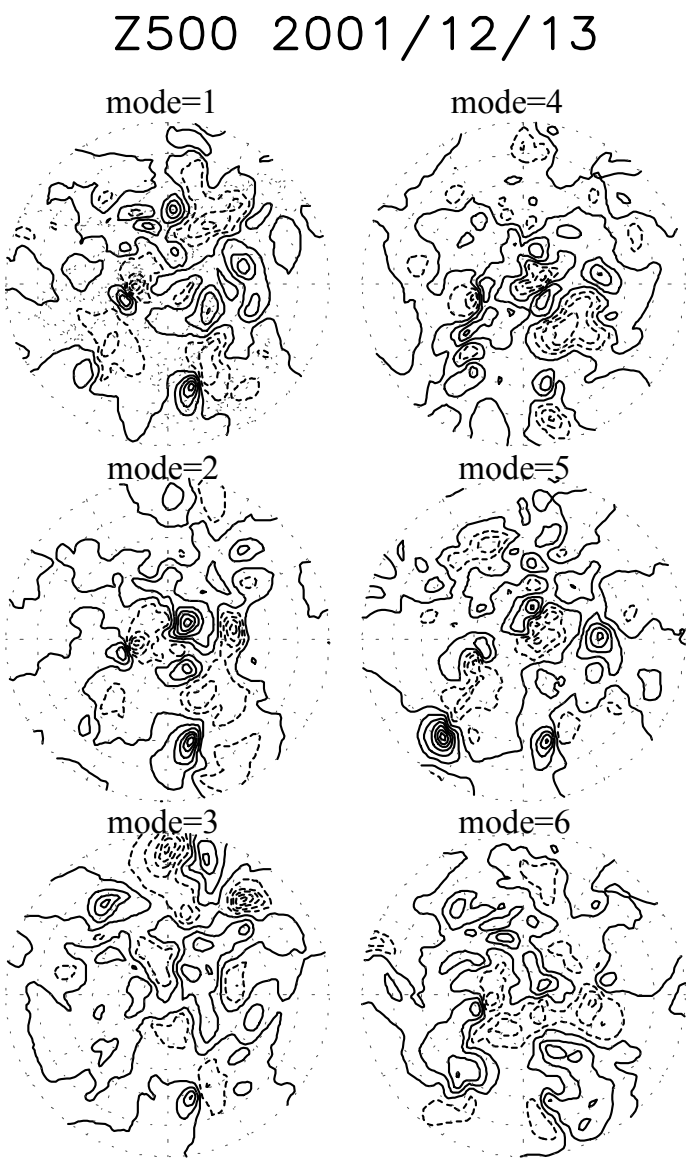

Figure 9: Horizontal distribution of the geopotential height of the obtained bred mode at 500hPa on 13 Dec. 2001 in a polar stereographic map north of 30°N. Top of each panel corresponds to the date line. Contour interval is 20 m. Dashed lines indicate negative values.

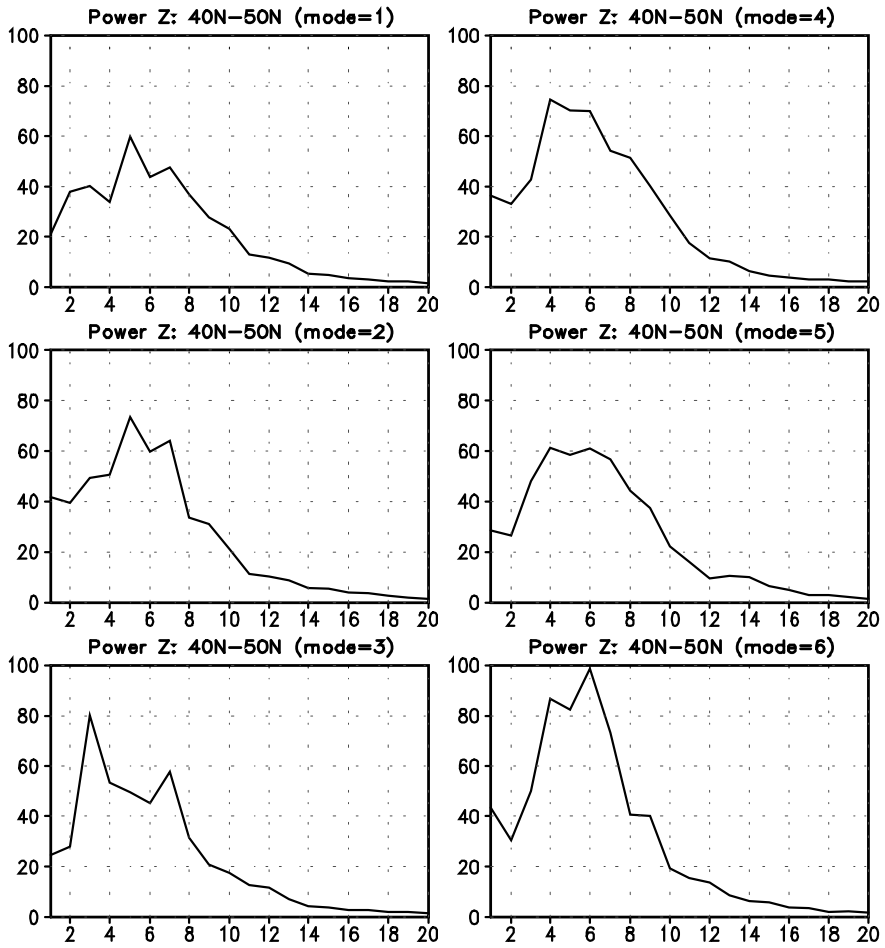

Figure 10: Zonal wavenumber spectrum of the amplitude of geopotential height at 300 hPa of the bred mode averaged over 40–50°N and a period of 23 days from 28 Nov. to 20 Dec. 2001. The abscissa is the wave number. Units of the ordinate are square meters.

5.2 Temporal evolution of bred modes

In this subsection, we examine the temporal evolution of the obtained NH bred mode. As described in Section 2.1, the amplitude of each NH bred mode at the initial time of forecast is specified such that the variance of the 500-hPa geopotential height of the mode, averaged north of 20°N, is 14.5% of the climatological variance.

Figure 11b shows the temporal variation of the amplification of each mode during initial one-day temporal integration starting every day. The magnitude of the amplification is assessed by the increment of the amplitude over one day. The same NWP model (GSM) used in the BGM cycle of the MRI-EPS was used to evaluate the temporal evolution of the bred mode. The operational NWP model used in Mukougawa *et al.* (2005) is referred to as the GSM0103. Note that the initial amplitude of each bred mode is about 15 m. Figure 11b shows that the average amplitude increment is about 6 m. The NH bred mode thus increases its amplitude by about 40% during the first day. However, it should be noted that the day-to-day variation of the amplification is very large. Moreover, the rate of amplification is almost the same among the bred modes: the amplitude increments, averaged over the experimental period, are 5.9, 6.3, 5.9, 6.3, 6.1, and 6.0 m for bred modes 1–6, respectively. We also confirmed that, as of 2001, the bred modes of the operational 1-month ensemble forecast of the JMA (GSM0103) evolve over time in a similar way (Figure 11a): the amplitude increments for each mode are 6.5, 5.8, 6.1, 6.2, 5.5, and 6.0 m, respectively.

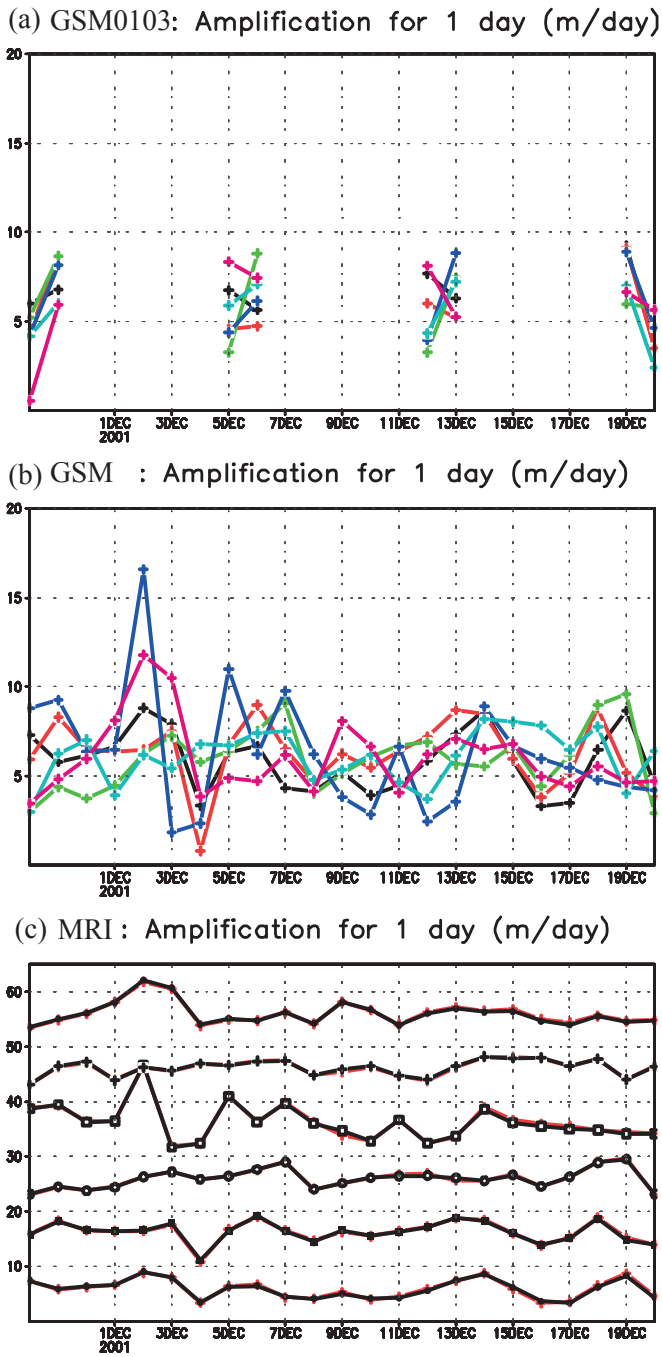

Figure 11: Amplitude increments (m) of each bred mode during the first one day. (a) The operational one-month ensemble forecasts as of 2001 (GSM0103). (b) Numerical forecasts are conducted by the GSM, and these forecasts are also used to obtain the bred mode. The amplitude is evaluated by the root-mean-square of the 500-hPa geopotential height variation poleward of 20°N. Each bred mode is designated by colors in (a) and (b): black for the first mode, orange for the second, yellow-green for the third, blue for the fourth, blue-green for the fifth, and magenta for the sixth. For panel (c), numerical forecasts were conducted by the

MRI-AGCM3.2 (black lines). The values for the GSM are also shown by red lines, which are the same as in panel (b). Note that 10(n – 1) m is added to the amplitude of the n-th bred mode in this panel to easily distinguish the amplitude of each mode.

6. Combination of the MRI-EPS and the MRI-AGCM3.2

6.1 MRI climate model (MRI-AGCM3.2)

Ensemble forecast experiments were performed by using a low-resolution version of the MRI-AGCM3.2 (Mizuta *et al.*, 2012). This model is based on the previous version of the JMA operational NWP model (GSM). Although several physical process schemes suitable for long-term integrations have been introduced into the model to facilitate its performance as a climate model, the fundamental part of the MRI-AGCM3.2 is common to the GSM, as described below. Results of long-term integrations with the MRI-AGCM3.2 have been verified from various points of view, and the model has been used for global warming research of the climate response to global warming conditions (e.g. Murakami *et al.*, 2011; Endo *et al.*, 2012). The model results are available for international use as one of the climate models in the Coupled Model Intercomparison Project Phase 5 (CMIP5; Taylor *et al.*, 2012). Furthermore, the model is used as the atmospheric component of the MRI-CGCM3 (Yukimoto *et al.*, 2011) and the earth system model MRI-ESM1 (Adachi *et al.*, 2013).

It is easy to configure experimental settings of the MRI-AGCM because it is developed for numerical experimental studies. Moreover, because the MRI-AGCM is a part of the earth system model, we can easily extend the experiments by coupling the other model components, such as the ozone chemical transport model.

The resolution of the model is set to be the same as that of the GSM used in the BGM cycle, which is TL159 (a grid interval of roughly 110 km) in the horizontal and 60 levels (top at 0.1 hPa) in the vertical. The dynamical framework is the same as that of the GSM, which is a hydrostatic primitive equation system that uses a spherical harmonic spectral transform method. The radiation scheme, the orographic gravity wave drag scheme, and the planetary boundary layer scheme are also the same as those in the GSM. Different physical process schemes are used for cumulus parameterization, cloud physics, land surface, and direct effects of aerosols. A new cumulus parameterization scheme has been developed, called the Yoshimura scheme (Yukimoto *et al.*, 2011; Yoshimura *et al.*, in preparation). The Tiedtke cloud scheme (Tiedtke, 1993) has been incorporated and is used in the model (Kawai, 2006). The model uses the land surface scheme of Hirai *et al.* (2007), which has been improved from the Simple Biosphere model (Sellers *et al.*, 1986) used in the GSM. More aerosol species are prescribed to calculate the direct effect of aerosols in detail. Details of the physical processes are described in Mizuta *et al.* (2012) and Yukimoto *et al.* (2011).

A normal-mode initialization scheme suitable for high-resolution global models (Murakami and Matsumura, 2007) has been applied to remove initial shock before integration of the MRI-AGCM3.2. The initial conditions for the land surface scheme are given by climatology with seasonal variation. The anomaly of the SST from the seasonally varying climatology is fixed

throughout the forecast experiments; the settings are the same as those used in the BGM cycle.

6.2 Temporal evolution of bred modes in various models

In this subsection, we examine the temporal evolution of the bred mode in the MRI-AGCM3.2. It should be noted that the BGM cycle generating the bred mode is based on the GSM, but not on the MRI-AGCM3.2. Because the adiabatic baroclinic instability process largely controls the temporal evolution of the bred mode, physical processes such as cumulus convection and radiation play only a secondary role. Hence, we can anticipate that the temporal evolution of bred modes is almost independent of the NWP model describing the evolution over time. Figure 11c compares the temporal variation of the amplification of each bred mode during the initial one-day temporal integration conducted by the MRI-AGCM3.2 (black lines) and by the GSM (red lines). This comparison confirms that the evolution over time is almost independent of the NWP model. We have therefore ascertained that the bred mode obtained with a BGM cycle based on the GSM is suitable for initial perturbations in ensemble forecast experiments based on the MRI-AGCM3.2.

6.3 Dependence of the temporal evolution of the bred mode on the analysis data

The bred mode obtained with the BGM cycle depends on the analysis field. As described in Section 3.1, we use the JRA-25/JCDAS analysis to compute the bred mode. It is thus natural to use the same analysis dataset (JRA-25/JCDA) to provide an unperturbed initial condition (control run) for the ensemble forecast experiment. However, there could be a demand for use of another reanalysis dataset, such as the European Centre of Medium-range Forecasting Reanalysis data (ERA-interim; Dee *et al.*, 2011) to conduct an ensemble forecast experiment. We therefore wished to confirm the consistency of the model by using different reanalysis datasets from JRA-25/JCDAS in advance. For this purpose, we compared the temporal evolution of the bred modes based on the JRA-25/JCDAS reanalysis and on the ERA-interim. Figure 12 compares the amplification of the bred modes during the first day of the ensemble forecasts based on each analysis during a period of 8 days from 10 to 17 December 2001. This comparison confirms that the amplification of the bred modes is almost independent of the analysis used in the ensemble forecast. It is thus ascertained that the ERA-interim reanalysis can also be used to provide an unperturbed initial condition for ensemble forecast experiments with initial perturbations represented by the bred mode of the BGM cycle. This fact also implies that the large-scale atmospheric state (especially in the troposphere), which controls the temporal evolution of the bred mode, is almost independent of the reanalysis datasets. In the following section, we examine the predictability of a SSW by using the ERA-interim reanalysis dataset for the unperturbed initial condition and the bred modes generated on the basis of the JRA-25/JCDAS dataset.

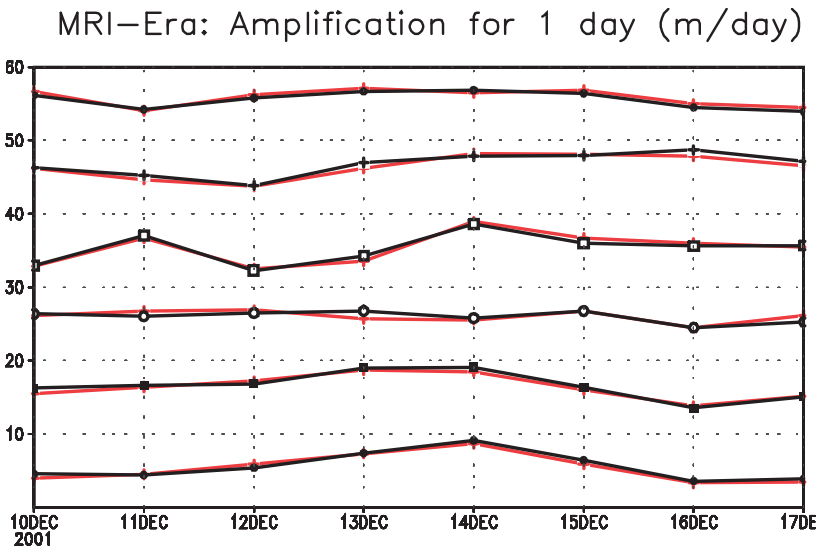

Figure 12: Same as in Figure 11c, except that the black lines indicate amplitude increments of bred modes obtained using the ERA-interim reanalysis data, and red lines for those obtained using the JRA-25/JCDAS reanalysis during the period from 10 Dec. to 17 Dec. 2001

7. Predictability of a SSW in the winter of 2001

Mukougawa *et al.* (2005) found, by using the operational one-month ensemble forecasting data of the JMA, that the SSW that occurred in December 2001 was predictable about two weeks prior to the date corresponding to the warming peak at 80°N of the zonal-mean temperature at 10 hPa. The predictable period was assessed from the spread of ensemble members (Figures 13a–d); the spread of forecasts starting on 12 and 13 December (Figure 13c) becomes much smaller than the spread of forecasts from 5 and 6 December (Figure 13b). The polar stratospheric temperature attains its maximum around 28 December. However, because the operational one-month forecast was conducted only twice a week (Wednesday and Thursday), a detailed examination of daily variations of the spread was not possible.

In this section, we examine the predictability of the SSW by using the newly developed MRI-EPS. We also investigate the dependence of the predictability on the NWP model that represents the temporal evolution of bred modes and also on the analysis dataset that provides the initial conditions of the forecast. Figure 13 shows the results of ensemble forecasts for the 10-hPa zonal-mean temperature at 80°N made by using the GSM0103 (Figures 13a–d), which was also used by Mukougawa *et al.* (2005); made by using the GSM (Figures 13e–h), which was used in the calculation of the BGM cycle for the MRI-EPS; and by using the MRI-AGCM3.2 (Figure 13i–l). Here, the red lines show the observations (NCEP/NCAR reanalysis). Each ensemble forecast was conducted with 26 ensemble members and was started every Wednesday and Thursday, as was the case in the operational 1-month forecast of the JMA in 2001. Note that the initial conditions for the GSM0103 were provided by the operational analysis of the JMA (GANAL), whereas those of the other models were provided by the JRA-25/JCDAS analysis. Thus, differences between the NWP model and the analysis dataset might affect the forecast. For the forecast that started on 28 and 29 November, no member of the GSM0103 predicted the occurrence of the SSW (Figure 13a), whereas several members predicted the SSW in the cases of the GSM and MRI-AGCM3.2 (Figures 13e and 13i). However, the forecasts that started on 5 and 6 December were very similar to each other (Figure 13b, f, and j). For the forecasts that started on 12 and 13 December, although all ensemble members of the forecasts predicted the occurrence of the SSW (Figures 13c, g, and k), the spread for the MRI-AGCM3.2 was relatively large (Figure 13k). For the forecast that started on 19 and 20 December, all the forecasts captured the occurrence of the SSW well, and the spreads were very small (Figures 13d, h, and l). Hence, the overall performances of the ensemble forecasts for the prediction of the SSW were very similar to each other.

We also conducted ensemble forecasts by using the GSM and the MRI-AGCM3.2 initialized every day. Figure 14 shows the ensemble mean (contour) and the standard deviation (shading) among the ensemble means for 10-hPa zonal-mean temperature at 80°N. Even in this

figure, there is no apparent difference between the two NWP models for the prediction of stratospheric polar temperatures: both ensemble mean values tend to increase after 20 December for the forecasts that started after 10 December; the forecasts that started after 13 December have the same peak value of 245 K around 27 December. Thus, both models predict the occurrence of the SSW almost two weeks in advance. However, when we closely examined both forecasts, we found that the performance of the GSM was slightly better than that of the MRI-AGCM3.2: the forecast of the GSM that started on 12 December predicts the peak temperature of the SSW well (Figure 14a). The performance of that model is almost the same as that of the MRI-AGCM3.2 that started on 13 December (Figure 14b).

We also examined the dependence of the ensemble forecast on the analysis dataset that provided the initial conditions by using the MRI-AGCM3.2. Figure 15 shows the ensemble forecasts for the polar stratospheric temperature based on the JRA-25/JCDAS reanalysis (Figure 15a) and the ERA-interim reanalysis (Figure 15b). Each forecast started from the period between 10 and 13 December, when the spread among the ensemble members rapidly decreased (Figure 14). It should be noted that the initial temporal evolution of the bred modes was almost independent of the reanalysis dataset, as shown in Section 6.3. It is apparent that the forecasts based on the ERA-interim reanalysis outperform those based on the JRA-25/JCDAS dataset; all ensemble members for the ERA-interim (JRA-25/JCDAS) reanalysis predict the occurrence of the SSW well for the forecasts that started after 11 December (13 December). This skillful performance may reflect the fact that the ERA-interim reanalysis produced a better representation of the stratospheric circulation compared with the JRA-25/JCDAS reanalysis. This fact is easily recognized by examination of the peak temperature of the 2001 SSW (not shown).

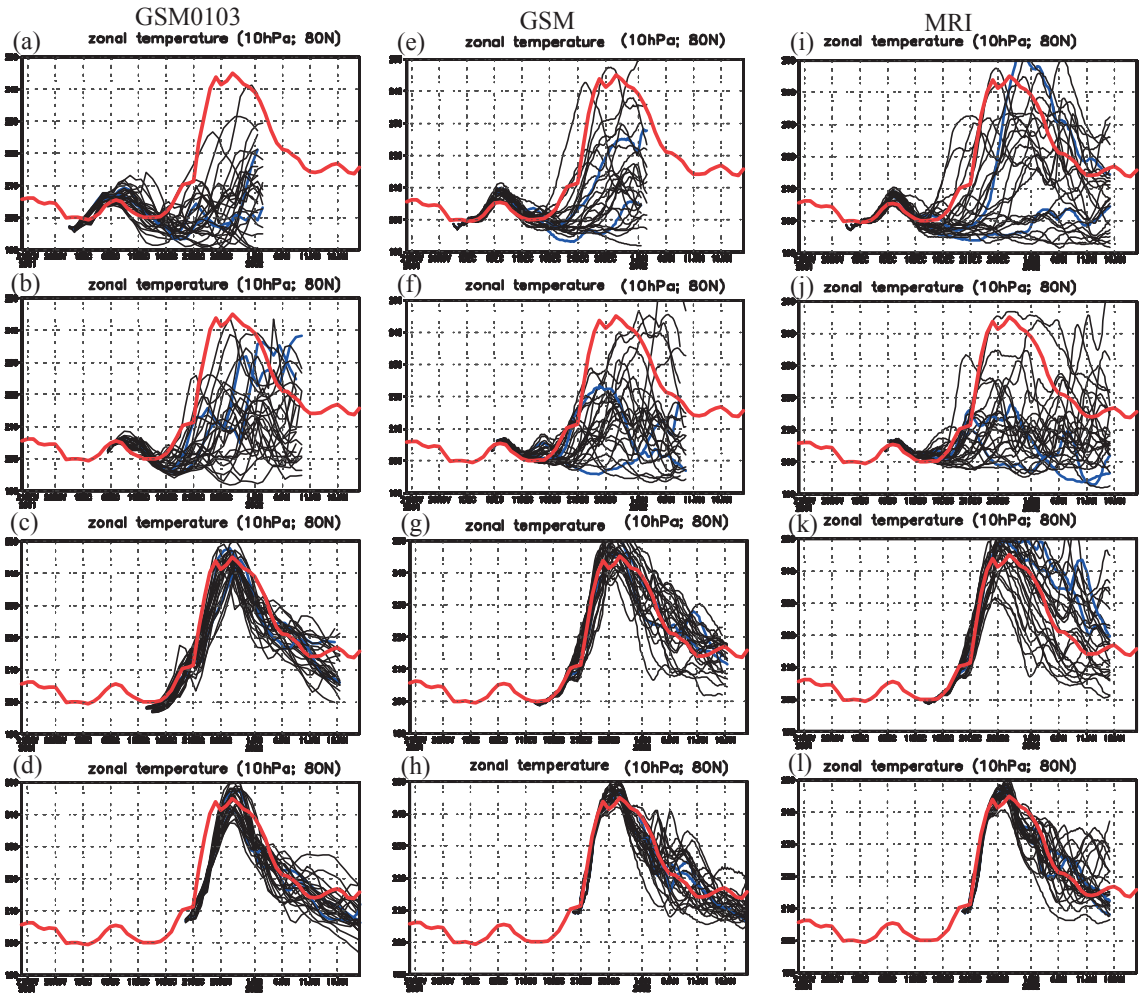

Figure 13: Temporal variation of 10-hPa zonal-mean temperature at 80°N from 20 Nov. 2001 through 20 Jan. 2002 for the analysis (red line) and ensemble forecasts (black lines). The forecasts started from (1st row) 28 and 29 Nov., (2nd row) 5 and 6 Dec., (3rd row) 12 and 13 Dec., and (4th row) 19 and 20 Dec. 2001. Blue lines indicate control runs. Panels (a–d) are forecasts made with the GSM0103, which were also used by Mukougawa *et al.* (2005). Panels (e–h) are forecasts made with the GSM, and panels (i–l) are those made with the MRI-AGCM3.2.

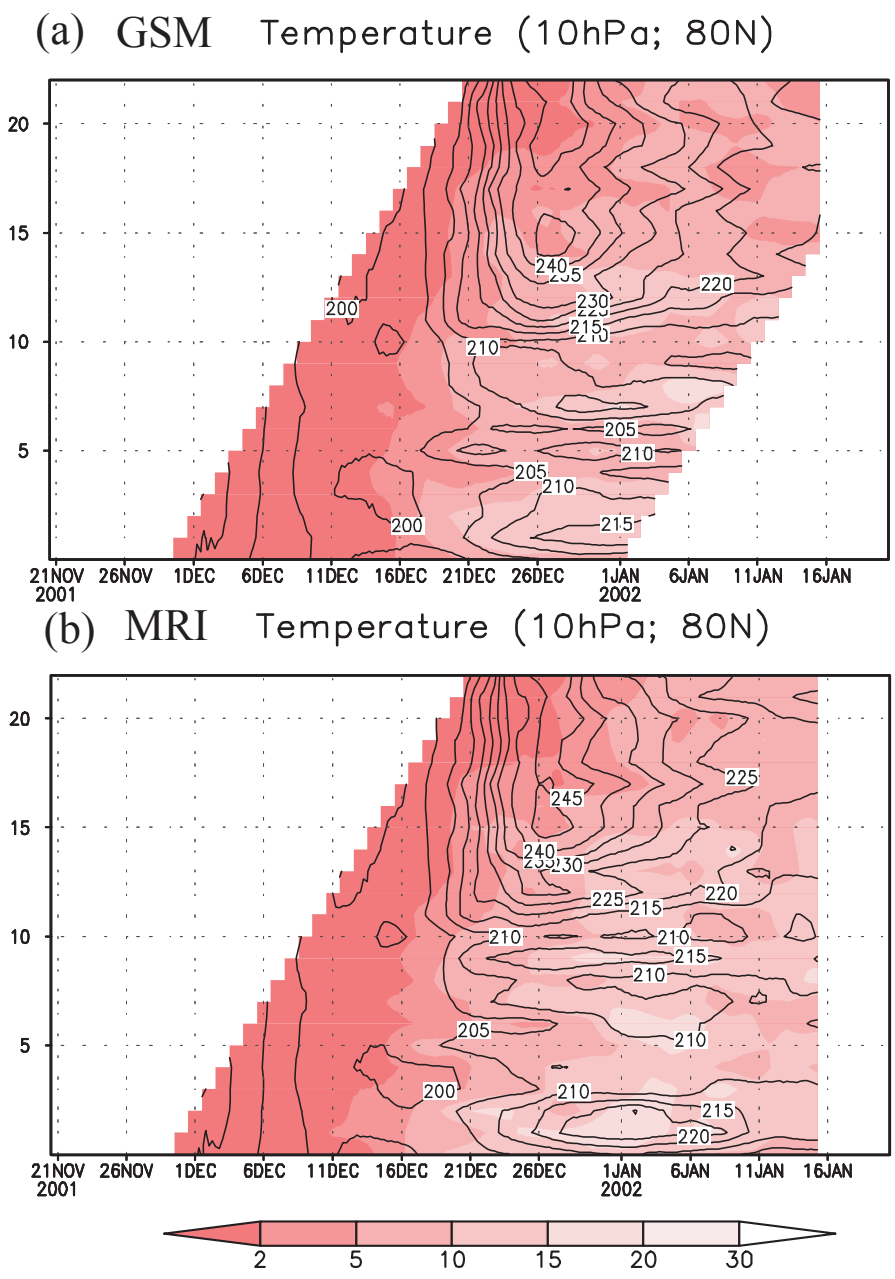

Figure 14: Ensemble mean (contour) and standard deviation (shading) of predicted 10-hPa zonal-mean temperature at 80°N made with (a) the GSM and (b) the MRI-AGCM3.2, initialized every day starting from 28 Nov. 2001.

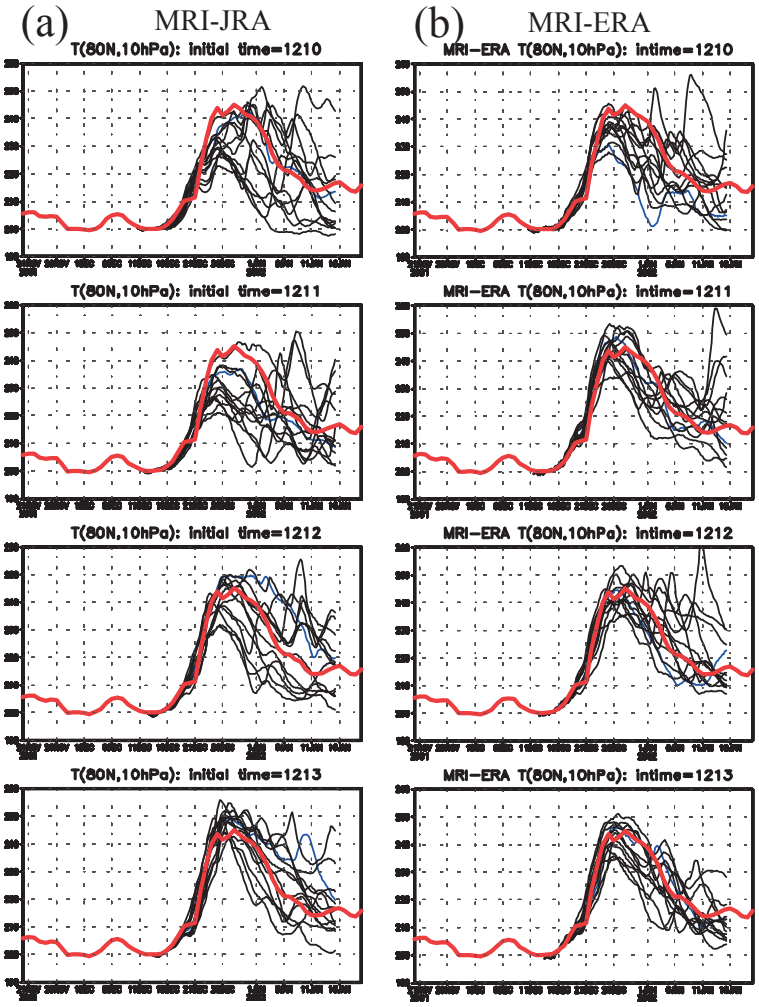

Figure 15: Same as in Figure 13, except that (a) the forecasts were made with the MRI-AGCM3.2 based on the JRA-25/JCDAS reanalysis and (b) the forecasts were made with the MRI-AGCM3.2 based on the ERA-interim reanalysis. Forecasts were initialized every day from 10 (the first row) to 13 (the fourth row) Dec. 2001.

8. Summary

A new ensemble prediction system, MRI-EPS, has been developed to promote the research activity of the MRI with respect to the predictability of climate and large-scale atmospheric motions. The BGM cycle, which is a key component of the MRI-EPS, can generate initial perturbations for the SH as well as for the NH and the TR. The fundamentals of the BGM method as well as the overview of the MRI-EPS have been described in this report. The BGM cycle system is based on the GSM, and we have confirmed that ensemble prediction experiments can be conducted flawlessly with the MRI-AGCM3.2 and the initial perturbations generated by the BGM cycle.

It is an important advancement for the MRI-EPS to be able to generate perturbations for the SH in addition to the NH and TR, which have already been generated by the operational one-month ensemble forecast system of the JMA. The skill of the Z500 ensemble forecasts for the SH made with ensemble predictions using the new SH initial perturbations has been found to be similar to those of NH predictions in the operational system.

We have also examined the spatio-temporal characteristics of the leading six bred modes during the period from 28 November to 20 December 2001, when a major SSW took place. Furthermore, we have conducted ensemble prediction experiments using two NWP models and two reanalysis datasets to examine the model dependency of the predictability of the SSW. The following results have been obtained with the foregoing examination:

1. The amplitude of geopotential height for the NH bred mode had two peaks at 300 hPa near 40–50°N and 80°N. The zonal wavenumber 6 component dominated the bred mode in the region around 40–50°N at 300 hPa.

2. The rate of amplification of the NH bred mode during the first day in the forecast was almost independent of the mode number. Although there were large day-to-day variations of the amplification rate, the bred mode increased its amplitude by about 40% on average during the first day.

3. The amplification rate of the NH bred mode was almost identical for the MRI-AGCM3.2 and GSM. Hence, bred modes generated by the BGM cycle of the MRI-EPS can also be used for initial perturbations of ensemble forecasts conducted by the MRI-AGCM3.2.

4. The temporal evolution of bred modes during the first day was also almost completely independent of the analysis dataset. Hence, although the bred mode of the MRI-EPS was generated based on the JRA25/JCDAS reanalysis dataset, the ERA interim reanalysis dataset can also be used to provide the unperturbed initial conditions for ensemble forecasts with the MRI-AGCM3.2.

5. With respect to the forecast of the SSW in 2001, ensemble predictions based on the ERA-interim reanalysis dataset outperformed those based on the JRA-25/JCDAS dataset. Hence, it

is useful to use the ERA-interim reanalysis dataset to provide the unperturbed initial conditions for ensemble predictions.

Table of Abbreviation

ACOR	:	Anomaly COrrelation Coefficient
AGCM	:	Atmospheric General Circulation Model
BGM	:	Breeding of Growing Mode
CMIP5	:	Coupled Model Intercomparison Project phase 5
COBE-SST	:	Centennial in-situ Observation-Based Estimates of the variability of Sea Surface Temperature and marine meteorological variables
CPD	:	Climate Prediction Division
D_{Z500}	:	Difference Z500 field between perturbed and control runs
ECMWF	:	European Centre for Medium-range Weather Forecasts
ERA-interim	:	European Centre for Medium-Range Weather Forecasts reanalysis data interim version
GANAL	:	(Japan Meteorological Agency) Global ANALysis data
GSM	:	(Japan Meteorological Agency) atmospheric Global Spectral Model
GSM0103	:	previous version of GSM whose forecasted data was used in Mukougawa et al.
JCDAS	:	Japan Meteorological Agency Climate Data Assimilation System
JMA	:	Japan Meteorological Agency
JMA-EPS	:	Japan Meteorological Agency -Ensemble Prediction System (operated in 2001 with GSM0103)
JRA-25	:	Japan ReAnalysis (25-year version)
LAF	:	Lagged Average Forecast
MRI	:	Meteorological Research Institute
MRI-EPS	:	Meteorological Research Institute -Ensemble Prediction System
MRI-ESM1	:	Meteorological Research Institute Earth System Model version 1
N	:	normalized perturbation
NCAR	:	National Center for Atmospheric Research
NCEP	:	National Centers for Environmental Prediction
NH	:	Northern Hemisphere
NMC	:	National Meteorological Center in the United States
No	:	orthonormalized perturbation
NTS	:	Abbreviation of NH+TR+SH
NT	:	Abbreviation of NH+TR
NuSDaS	:	Numerical weather prediction Standard Data-set System (in Japan Meteorological Agency)
NWP	:	Numerical Weather Prediction
PDF	:	Probability Distribution Function

RMSE	:	Root Mean Square Error
Pre-BGM	:	a cycle which are performed previously for BGM cycle
SAM	:	Southern Annular Mode
SH	:	Southern Hemisphere
SiB	:	Simple Biosphere Model
SPREAD	:	Ensemble spread
SST	:	Sea Surface Temperature
SSW	:	Stratospheric Sudden Warming
SV	:	Singular Vector
SVD	:	Singular value decomposition
T_0	:	start time of BGM cycle shown in Fig.2
T_{p0}	:	start time of pre-BGM cycle shown in Fig.2
TR	:	Tropical Region
Z500	:	500-hPa geopotential height
χ200	:	velocity potential at 200 hPa level

Appendix（付録）

以下では、2013 年現在の MRI 計算機システムユーザーが本 BGM アンサンブル実験システムを利用する際に必要な技術情報を補足して記す[6]。

A1 実験環境の準備

A1.1 BGM システムディレクトリ

圧縮されたシステムファイル MRIBGM.tar.gz を気候研究部の RAID ディスク（以下、システムディスクと呼ぶ。場所は http://graphsv/User/cl/syabu/BGM/ を参照）から MRI スパコンシステム(front)のユーザーディレクトリ(/home3 や/home1）以下の適当なディレクトリにコピーし、以下のコマンドで圧縮を解く（$ はシェルのプロンプト、以下同様）：

$ gzip -dc MRIBGM.tar.gz | tar -xvf -

BGMディレクトリが作成される。これを以下BGMシステムディレクトリ（略号$BGMDIR）と呼ぶ。ディレクトリ構成は以下のとおり：

```
$BGMDIR      :（トップディレクトリ、実験シェルスクリプトを含む）
  /Module    : 実行モジュール（ソースなどを含む）
  /Const     : 定数ファイル
  /Sh        : 実行（子）シェル
  /Tool      : BGM 関係ツール
```

A1.2 BGM データディレクトリ

front の /work 上の適当なディレクトリ（以下$WBGMDIR）を、実験の入出力データの格納場所とする。標準的なディレクトリ構成は以下のとおり：

```
$WBGMDIR     :（トップディレクトリ）
  /Data      :（入力データディレクトリ）
    /JRA     : 大気再解析値（JRA-25/JCDAS）
    /lfin_lnd: 陸面気候値（気象庁気候情報課オフライン解析に基づく）
    /COBE    : 海面水温・海氷解析値（COBE-SST）
    /Ptbnh*  : BGM（本）サイクル開始時に与える摂動データ
               （北半球サイクル用、*=4 or 25 は実験の摂動モード数）
    /Ptbsh*  :（同上、ただし南半球サイクル用）
    /Ptbtro  :（同上、ただし熱帯サイクル用）
```

[6] 本実験システムの入出力データは気象庁 NuSDaS 形式であるが、本付録では NuSDaS についての知識を極力前提としない記述とした。（NuSDaS に関する脚注は必ずしも理解を必要としない。）

/$EXPDIR　：BGM サイクル実験ごとの出力ディレクトリ
（ディレクトリ名は、A2 の実験シェルスクリプトで指定）
/Ptbnh　：BGM サイクル実験で得た北半球摂動データ
/Ptbsh　：同上、ただし南半球摂動データ
/Ptbtro　：同上、ただし熱帯摂動データ
/LFIN　：アンサンブル初期値データ
/FCST　：アンサンブル予報値データ

各種解析データは $WBGMDIR/Data と同じディレクトリ構成で、システムディスクに置いているので、そこから $WBGMDIR にコピーする。JRA と lfin_lnd は年別のディレクトリになっているので、実験に使う期間分だけで構わない。（なお、lfin_lnd は 3.1 節で述べたように実態は気候値であるが、形式上は日付のついた解析値のように扱う。） 出力ディレクトリ（$EXPDIR, LFIN, FCST）は、実験実行時に自動的に作成されるので、予め準備する必要はない。

A1.3 BGM 作業ディレクトリ

front の /short 上の適当なディレクトリ（以下$SBGMDIR）を、実験の作業ディレクトリとして利用する。標準的なディレクトリ構成は以下のとおり：

$SBGMDIR　：（トップディレクトリ）
/$EXPDIR　：サイクル実験ごとの作業ディレクトリ
（ディレクトリ名は、A2 の実験シェルスクリプトで指定）
/PRE##p　：プレサイクル実験時のモード(##=01,02,…)ごとの
作業ディレクトリ
/LFIN　：アンサンブル初期値作成時の作業ディレクトリ
/FCST　：アンサンブル予報実験時の作業ディレクトリ

これらのディレクトリも、実験実行時に自動的に作成されるので、予め準備する必要はない。

A1.4 計算済み BGM 摂動データ

実験に必須なデータではないが、システムディスクの Ptb ディレクトリには、本研究において計算した北半球・南半球（各 25 モード）と熱帯（２モード）の BGM 摂動データが保存されている。それぞれ　Ptb/NH25/Ptbnh 、Ptb/SH25/Ptbsh および Ptb/TRO/Ptbtr 以下に配置され、たとえば、ある日の北半球の 12UTC 時刻の摂動データファイルは、

ptb12/（日付）/ptb_cycl12.nus　（12UTC 時刻、サイクル継続用）
/ptb_fcst12.nus　（　同上、　予報実験用）

によって参照することができる。本原稿執筆時現在では、2001 年 10 月から 2013 年３月の各日についての計算値がある。A2 で述べる、サイクル実験の開始時の適当な摂動データがない場合は、サイクル継続用の方を利用することができる。また、予報実験用の方は、この期間のアンサンブル予報実験のための摂動初期値作成（A2.4）に直接用いることができる。

A2 実験の実行手順

A2.1 プレサイクル

北半球または南半球 BGM サイクルの実験開始時の適当な摂動データがない場合に実施する。実験シェルスクリプトは $BGMDIR/pre_nh*p.sh （北半球用、*=4 or 25 は計算モード数で、いずれかを用いる）または $BGMDIR/pre_sh*p.sh （南半球用）で、テキストエディタで開いて、最初の方の以下の部分を適宜編集する：

```
#--- set belows ------------------------------------------------------------
GRP=cl                              # user parameters on MRI-system
UID=syabu
ACCOUNT=K0211

HOMEDIR=/home3/${GRP}/${UID}            # (alias dir.name
WOMEDIR=/work/${GRP}/${UID}#     ; no need to edit)
SOMEDIR=/short/${GRP}/${UID}  #

BGMDIR=${HOMEDIR}/BGM      # BGM system dir.
SBGMDIR=${SOMEDIR}/BGM     # BGM working dir.
CENDDATE=20040106                # end date of pre-cycle
                                 #     (! MUST BE : day of CENDDATE    >=6 )
# set analysis data dir.
ANALDIR=${WOMEDIR}/BGM/Data
# set first Ptb.dir. for BGM (main) cycle
PTB1DIR=${WOMEDIR}/BGM/Data/Ptbnh4
# ----------------------------------------------------------------------------
```

GRP, UID および ACCOUNT は、MRI システムのグループ名、ユーザー名、ジョブの実行アカウント番号をそれぞれ指定する。BGMDIR,SBGMDIR には、それぞれ BGM システムディレクトリ、BGM 作業ディレクトリ名を指定する。CENDDATE はプレサイクルの終了日付であり、最も古い開始日から始めるモード（第２章 Figure 2 参照）のプレサイクルに

必要なデータが前月のものになることを避けるため、４モード版は 6 日以降、25 モード版は 27 日以降（で月末までのいずれか）の日付を指定しなければならないことに注意。ANALDIR には、準備した解析データのディレクトリを指定する。PTB1DIR は、プレサイクルの結果（= 本サイクルの最初に用いる摂動データ）を保存する場所を指定する。なお、HOMEDIR, WOMEDIR, SOMEDIR は、/home3, /work, /short の各ディレクトリ下のユーザーのトップディレクトリを表すエイリアスで、設定は不要。他の実験シェルスクリプトもそうであるが、上記のように雛形としては

BGM システムディレクトリ　$BGMDIR　= /home3/${GRP}/${UID}/BGM
BGM データディレクトリ　　$WBGMDIR = /work/${GRP}/${UID}/BGM
BGM 作業ディレクトリ　　$SBGMDIR = /short/${GRP}/${UID}/BGM

をそれぞれ仮定しているが、必ずしもこのとおりでなくてもよい。

上記の編集の終了後、プレサイクルを通常のコマンドで実行する。たとえば、４モード版の北半球用プレサイクルでは、$BGMDIR にカレントディレクトリを移動して、

$ ./pre_nh4p.sh

とする。すると、$SBGMDIR/PRE##p (##=01～04：摂動モード番号) という作業ディレクトリが作成され、その下にプレサイクル実験の環境が整えられ、次いで、各モードのプレサイクルが順に $BGMDIR/pre_1p.sh を呼び出して実行される。pre_1p.sh では、第３章の Figure 3 に示したように、llsub_bgm_nh1p と llsub_bgm_nh1 （北半球用の場合）というジョブコントロールファイル(JCF) を llsubmit して、プレサイクルを制御している。各サイクル実行中は 10 分ごとに、

+++01p

のように、現在行われているプレサイクルのモード番号が標準出力（通常、端末画面）に表示される。（特に 25 モード版は、最後のモードに達するまで 1 日以上かかるので、気長に待つこと。なかなか次のモードに移らない場合は、一部のジョブがホールドされていることが多いので、llhold -r で解放する。）すべてのサイクルが終了すると、

1st 4mode ptb.s in $CENDDATE are created.

といったメッセージが標準出力に表示され、

${PTB1DIR}/ptb12/${CENDDATE}/ptb_cycl12.nus ディレクトリに BGM サイクル開始用の各モードの摂動データが作成される[7]。

A2.2 北半球（南半球）BGM サイクルの実行

実験シェルスクリプトは $BGMDIR/pre_nh*.sh （北半球用、*=4 or 25）または $BGMDIR/pre_sh*.sh （南半球用）で、テキストエディタで開いて、最初の方の以下の部分を適宜編集する：

[7] なお、プレサイクルや BGM サイクル（A2.2,A2.3）中の各ジョブの実行ログファイルは BGM 作業ディレクトリ下の Sh/Log（このプレサイクルの例では、${SBGMDIR}/PRE##p/Sh/Log）に出力される。プレサイクルが異常終了した場合に参照するとよい。

```
#--- set belows ------------------------------------------------------------
# user parameters on MRI-system
GRP=cl
UID=syabu
ACCOUNT=K0211

HOMEDIR=/home3/${GRP}/${UID}        # (alias ; no need to edit)
WOMEDIR=/work/${GRP}/${UID}
SOMEDIR=/short/${GRP}/${UID}

# first target date of cycle = cycle start date +1day (format YYYYMMDD)
C1DATE=20040107
#C1DATE=20040113        # re-start
# last target date of cycle = cycle end date
CENDATE=20040131
# name of experiment (identifier)
EXPNAME=TESTNH4

BGMDIR=${HOMEDIR}/BGM       # BGM system dir.
WBGMDIR=${WOMEDIR}/BGM  # BGM work dir. (in /work)
SBGMDIR=${SOMEDIR}/BGM     # BGM work dir. (in /short)

# data directories
DATADIR=${WBGMDIR}/Data                  # analysis data top dir.
P1STDIR=${WBGMDIR}/Data/Ptbnh4/ptb12 # 1st. perturbation (pre-built)
#P1STDIR=${WBGMDIR}/${EXPNAME}/Ptbnh/ptb12 # 1st.perturbation (re-start)
PTBDIR=${WBGMDIR}/${EXPNAME}/Ptbnh                  # Ptb. save dir.
#-------------------------------------------------------------------------
```

C1DATE には、サイクルの最初の目標日付（最初の摂動を計算する日付＝サイクル開始日＋１日）を指定し、CENDATE には、サイクルの終了日付（最後の摂動計算日付）を指定する。EXPNAME は、サイクル実験を特定する実験名で、任意の文字列を設定する。DATADIR には解析データの置き場所（トップディレクトリ）を、また P1STDIR には A2.1 のプレサイクルや過去の同様のサイクル実験などによって用意した、サイクル開始時の摂動データの（ptb12）ディレクトリを、それぞれ指定する。PTBDIR には、BGM サイクルでこれから計算される各日時の摂動データが保存されるディレクトリを指定する。その他の

シェル変数については、A2.1 のプレサイクルと同様。

上記の編集の終了後、BGM サイクルを実行する。たとえば北半球４モード版の場合、$BGMDIR にカレントディレクトリを移動して、

$ ./pre_nh4.sh

実行中はスクリプトの CENDDATE で指定した日時まで、24（実験）時間ごとに、llsub_bgm_nh4 という JCF ファイルが llsubmit され、サイクルが制御される（第３章の Figure 4 を参照）。計算結果の摂動ファイルは ${PTBDIR} ディレクトリ以下に、

ptb12/（日付）/ptb_cycl12.nus　（ 12UTC 時刻、サイクル継続用）
　　/ptb_fcst12.nus　（　同上、　予報実験用）
ptb00/（日付）/ptb_cycl12.nus　（ 00UTC 時刻、サイクル継続用）

のように作成される。

A2.3 熱帯 BGM サイクルの実行

実験シェルスクリプトは $BGMDIR/pre_tro.sh であり、テキストエディタで開いて、A2.2 と同様に最初の方の

#--- set belows ----------

と

#----------

で囲まれた部分を適宜編集する。各設定項目（シェル変数）は、 A2.2 の北（南）半球サイクルの場合と同じである。P1STDIR に格納場所を指定する、熱帯 BGM サイクル開始時の摂動データについては、第３章でも述べたように、過去の同様な BGM サイクルの結果があればそれを用いるが、なければ、A2.2 で得た北半球 BGM 摂動データを、A3.1 で後述するツールを用いて熱帯用（ダミー）摂動データに変換して用意する。

編集の終了後、BGM サイクルを通常のコマンドで実行する（$BGMDIR で）:

$ ./pre_tro.sh

スクリプトの CENDDATE で指定した日時まで、24（実験）時間ごとに、llsub_bgm_tro という JCF ファイルが llsubmit され、サイクルが制御される（第３章の Figure 5 を参照）。計算結果の摂動ファイルは

${PTBDIR}/ptbtr/（日付）/ptbtro_cycl12.nus（12UTC 時刻、サイクル継続用）
　　/ptbtro_fcst12.nus （　同上、　予報実験用）

のように作成される。

A2.4 アンサンブル予報実験用モデル初期値の作成

$BGMDIR/make_lfin_*.sh（*=4 or 25：摂動モード数）により、予報モデル用のコントロールおよび摂動初期値を作成する。最初の以下の部分を適宜編集する：

#--- set belows --- (! also account_no above) ----------

```
# user parameters on MRI-system
GRP=cl
UID=syabu

HOMEDIR=/home3/${GRP}/${UID}            # (alias ; no need to edit)
WOMEDIR=/work/${GRP}/${UID}
SOMEDIR=/short/${GRP}/${UID}

BGMDIR=${HOMEDIR}/BGM      # BGM system dir.
WBGMDIR=${WOMEDIR}/BGM  # BGM work dir. (in /work)
SBGMDIR=${SOMEDIR}/BGM     # BGM work dir. (in /short)

INITLIST=${BGMDIR}/initlist.txt  # external configuration file
                                 #      in which init.dates are listed
# name of experiment (identifier)
#EXPNAME=PTB_NTS   # +- (NH+TR+SH) Ptb.
EXPNAME=PTB_NT                   # +- (NH+TR) Ptb.

# directory where initial data files for forecast model are stored
OUTDIR=${WBGMDIR}/LFIN/${EXPNAME}

# directories of analysis data
DATADIR=${WBGMDIR}/Data
ANL_P0=${DATADIR}/JRA                                          # atmosphere
ANL_L0=${DATADIR}/lfin_lnd                                     # land surface
ANL_S=${DATADIR}/COBE/Ks.Latest/Sst/sst_anal.nus               # sea surface

# directories of perturbation data
# (if no ptb. data ,null directory is enough)
PTBNH=${WBGMDIR}/TESTNH4/Ptbnh/ptb12
PTBTR=${WBGMDIR}/TESTTRO/Ptbtr/ptbtr
PTBSH=${WBGMDIR}/TESTSH4/Ptbsh/ptb12

# NuSDaS type3 : choose 'NONE' if no ptb. data exists
FPBNH='FPBN' # NH Ptb.    ('FPBN' or 'NONE')
FPBTR='FPBT'  # TR Ptb.    ('FPBT' or 'NONE')
```

```
FPBSH='NONE' # SH Ptb.   ('FPBS' or 'NONE')
WRKDIR=${SBGMDIR}/LFIN       # working dir.
#-------------------------------------------------------------------------
```

最初に、この前の部分（JCF 部分）にある @account_no= の行に、自分の研究課題の課金番号を記入しておく。GRP から SBGMDIR までは、A2.2 と同様。INITLIST には、初期値日付のリストを次の例のように記入した、外部日付リストファイルを指定する：

```
initdate list : format= YYYYMMDD (HH=12) ; last line must be "end"
20040130
20040131
end
```

（2004 年 1 月 30 日と 31 日が対象の例。最初と最後の行は変更しないこと。）
EXPNAME には、作成する初期値のタイプを特定する文字列を指定する。第 4 章で説明したような、北半球・熱帯・南半球の各摂動の組み合わせの違いなどを区別するような目的に使用できる。OUTDIR は、作成される初期値 (LFIN) データの保存ディレクトリを指定する。ANL_P0, ANL_L0, ANL_S はそれぞれ大気、陸面、海面の解析データのディレクトリを指す（${DATADIR} 以下に標準的にデータが配置されていれば、編集不要）。PTBNH, PTBTR, PTBSH には、それぞれ北半球、熱帯、南半球 BGM 摂動データの格納ディレクトリを指定する。ただし、３つの領域摂動データの一部によってアンサンブル初期値を作成する場合は、用いない領域に対しては何も指定しなくてもよい。FPBNH, FPBTR, FPBSH では、北半球・熱帯・南半球各領域の摂動データの利用の有無を指定する。各領域について、利用する場合はそれぞれ'FPBN', 'FPBT', 'FPBS' の文字列を与え[8]、利用しない場合は代わりに 'NONE' の文字列を指定する。（上記の例では、北半球と熱帯の摂動のみを用いる：第 4 章の NT 実験に対応。）WRKDIR は初期値作成のための作業ディレクトリである。

編集が終了したら、以下のように llsubmit 実行する（$BGMDIR で）：

```
$ llsubmit make_lfin_4.sh          （４モード版の場合）
```

ジョブが終了すると、$WBGMDIR/LFIN ディレクトリに、

```
${EXPNAME}/（日付）/LFIN_nus
```

のように、各日 12UTC のアンサンブル初期値データが作成される。

A2.5 アンサンブル予報実験の実行

実験シェルスクリプトは、４摂動モードの場合は $BGMDIR/pre_fcst1.sh である。25 摂動モードの場合は、コントロール予報および最初の４モードの摂動予報（01p～04m）には $BGMDIR/pre_fcst1.sh を用い、他の摂動予報には $BGMDIR/pre_fcst2.sh を用いる。それぞれテキストエディタで開いて、最初の方の以下の部分を適宜編集する。

[8] なお、これらの文字列はそれぞれの摂動データの NuSDaS 第３種別(type3)にあたる。

まず、pre_fcst1.sh について：

```
#--- set belows ------------------------------------------------------------
# user parameters on MRI-system
GRP=cl
UID=syabu
ACCOUNT=K0211

# forecast period (hour)
KTEND=816
# experiment name (identifier)
#EXPNAME=PTB_NTS   # (NH+TR+SH =Global Ptb.)
EXPNAME=PTB_NT                  # (NH+TR Ptb. ,no SH Ptb.)

HOMEDIR=/home3/${GRP}/${UID}            # (alias ; no need to edit)
WOMEDIR=/work/${GRP}/${UID}
SOMEDIR=/short/${GRP}/${UID}

BGMDIR=${HOMEDIR}/BGM      # BGM system dir.
WBGMDIR=${WOMEDIR}/BGM  # BGM work dir. (in /work)
SBGMDIR=${SOMEDIR}/BGM     # BGM work dir. (in /short)

INITLIST=${BGMDIR}/initlist.txt  # external configuration file
                                 #      in which init.dates are listed

INITDIR=${WBGMDIR}/LFIN/${EXPNAME}                    # initial data dir. (made by
make_lfin.sh)
FOUTDIR=${WBGMDIR}/FCST/${EXPNAME}         # output dir. (forecast data)
#-------------------------------------------------------------------------------
```

KTEND には予報期間を時間で指定する。ただし仕様により、指定できる最長は 816 時間（34 日）。EXPNAME は実験名を表すが、上記の例では、A2.4 の初期値作成時と同じ文字列を想定している。INITLIST は A2.4 での説明同様、初期日付リストファイルを指し示す（A2.4 の初期値作成時と同じファイルを指してもよい）。INITDIR には、A2.4 で作成した初期値データのディレクトリを指定する。FOUTDIR は、予報値ファイルの出力ディレクトリである。その他の行については、A2.2 と同様。

編集が終わったら、$BGMDIR 上で、

$ ./pre_fcst1.sh

によって実行すると、１初期日ごとに、コントロールおよび摂動予報ジョブが順に投入され、すべてのメンバーの予報が終了すると、初期日を更新して、再び予報ジョブを順次 llsubmit してゆく。予報結果の気圧指定面（p-面）ファイルは、${FOUTDIR}/（初期日付）/（メンバー名）/fcst_p.nus のように、初期日・予報メンバーごとに出力される。

なお、p-面ファイルに収められる予報データは 1.25° の等間隔緯経度データで、指定気圧レベル数は 23（地表面および、1000, 925, 850, 700, 600, 500, 400, 300, 250, 200, 150, 100, 70, 50, 30, 20, 10, 7, 5, 3, 2, 1 hPa の各気圧レベル）。予報要素は、東西風(U)、南北風(V)、気温(T)、高度(Z)、海面更正気圧(PSEA)の他、（必ずしも全気圧レベルで定義されていないが）以下の要素が保存される：湿数(TTD)、鉛直速度(OMG)、渦度(VOR)、速度ポテンシャル(CHI)、流線関数(PSI)、時間積算雨量(RAIN)、雲水量(CWC)、各層雲量(CVR)、全雲量(CLA)、下層雲量(CLL)、中層雲量(CLM)、上層雲量(CLH)。[9]

25 モード版（51 メンバーアンサンブル予報実験）の場合は、（MRI システムでの１ユーザーの最大同時投入ジョブ数を考慮して、）摂動予報については最大４モード（８メンバー予報）ずつに分けて予報を実行する。第１から第４モードについては、４モード版と同様に pre_fcst1.sh を編集して実行する。第５モード以降は、pre_fcst2.sh の方を用いる。編集方法は pre_fcst1.sh とほとんど同じだが、以下の部分を追加して設定する：

```
### modes selection (COMMENT-OUT ONE OF BELOW LINES)
MEMGRP=2                # 05p - 08m
#MEMGRP=3     # 09p - 12m
#MEMGRP=4                # 13p - 16m
#MEMGRP=5                # 17p - 20m
#MEMGRP=6                # 21p - 24m
#MEMGRP=7                # 25p - 25m
```

MEMGRP は、予報実験を行うメンバーの群を指定する。６行のうち１行だけをコメントアウトすると、その１行の# 以下に記されているメンバーの予報を指定したことになる（上記の例では 05p から 08m）。実行コマンドやその予報結果のディレクトリについては pre_fcst1.sh での説明と同様。まとめると、25 モード版の予報実験では、まず pre_fcst1.sh でコントロール予報と 01p～04m 摂動予報を実行し、次いで、MEMGRP を２から７に順に変えながら、pre_fcst2.sh を計６回順次実行する。

A2.6 予報データの GrADS データ形式への変換

A2.5 の予報実験によって出力される予報値（p－面）データは、気象庁 NuSDaS 形式にな

[9] ここで示した気圧（レベル）や予報要素名（括弧内の文字列）は、NuSDaS 形式である p-面予報データの GrADS 化ツール（A3.2 の プログラム rdnus2gr）によるデータ変換において、変換対象データを指定する際に用いられる。

っている（fcst_p.nus)。気象関係のデータ描画でよく使われる GrADS ソフトウェアの標準データ形式（４バイト実数のバイナリデータ、以下 GrADS 形式と呼ぶ）にするには、A3.2 で後述する rdnus2gr のような変換プログラムが必要である。ここでは、このプログラムを用いた変換例を示す。

以下は、BGM 関連ディレクトリ（$BGMDIR/Tool）にある変換シェルスクリプト rdnus2gr_ens.sh の前半の設定部分の抜粋である：

```
#-----------------------------------------------------------------
# set belows
#-----------------------------------------------------------------
GRP=cl              # user parameters on MRI-system
UID=syabu           # ! also modify @account_no above

HOMEDIR=/home3/${GRP}/${UID}          # (alias ; no need to modify)
WOMEDIR=/work/${GRP}/${UID}
SOMEDIR=/short/${GRP}/${UID}

BGMDIR=${HOMEDIR}/BGM      # BGM system dir.
TOOLDIR=${BGMDIR}/Tool                  # BGM tool dir.
WORKDIR=${SOMEDIR}/Rdnus2gr          # work dir.

PGM=${TOOLDIR}/rdnus2gr                 # convert program

INITLIST=${BGMDIR}/initlist.txt  # external configuration file
                                        #      in which init.dates are listed

OUTDIR=${WORKDIR}              # output directory
DATFILE=zuvtdo_ens                      # filename of output (GrADS) datafile
MSKFILE=${TOOLDIR}/mask200201.dat     # (topographical) mask data file
                                        # (not used ,if fmask='nomask')
MEMBERS="00 01p 01m 02p 02m 03p 03m 04p 04m"       # ensemble forecast members
#MEMBERS="00 01p 01m 02p 02m 03p 03m 04p 04m 05p 05m 06p 06m 07p 07m 08p 08m 09p
09m 10p 10m 11p 11m 12p 12m 13p 13m 14p 14m 15p 15m 16p 16m 17p 17m 18p 18m 19p 19m
20p 20m 21p 21m 22p 22m 23p 23m 24p 24m 25p 25m"       # ensemble forecast members

DIRFCSTP=${WOMEDIR}/BGM/FCST/PTB_N     # NuSDaS forecast data (fcst_p.nus) dir.
```

```
# namelist parameters ---------------------------------------------------------
NAMGR="fname='temp.dat' ,xdef=288 ,ydef=145 ,zdef=1 ,tdef=1"
NAMSK="fmask='nomask' ,lvls=23 ,vlvl='SURF','1000','925 ','850 ','700 ','600 ','500 ','400 ','300
','250 ','200 ','150 ','100 ','70  ','50  ','30  ','20  ','10  ','7   ','5   ','3   ','2   ','1   '"
NAMVR="iznl=0  ,nvar=28  ,celm='PSEA  ','Z       ','Z       ','Z       ','Z       ','Z       ','Z
','Z       ','Z       ','Z       ','Z       ','Z       ','Z       ','Z       ','Z       ','Z       ','Z
','Z       ','Z       ','Z       ','Z       ','Z       ','U       ','V       ','T       ','TTD     ','OMG
' ,clvl='SURF','1000','925 ','850 ','700 ','600 ','500 ','400 ','300 ','250 ','200 ','150 ','100 ','70  ','50
','30 ','20  ','10  ','7   ','5   ','3   ','2   ','1   ','ALL ','ALL ','ALL ','ALL ','ALL '"
#! idate is set in initdate loop
NAMDT0="idate=YYYY,MM,DD,HH,0 ,nkt=0,ikt=0,816,6"
#! member is set in member loop
NAMNS0="type1='_SF1LLPP' ,type2='FCSV' ,type3='STD1' ,member='MEMB'"
NAMGL="ig2l=0"
# -----------------------------------------------------------------------------
```

この例は、816 時間予報した 9 メンバーの、初期値および 6 時間ごとの全指定面における予報値を、地上気圧／高度（PSEA/Z）、東西風（U）、南北風（V）、気温（T）、湿数（TTD）、および鉛直速度（OMG）について、変換し出力するものである。

まず最初に、この部分より上の@account_no=の行に、各々の研究課題の課金番号を記述しておく。WORKDIR には、このプログラム用の作業用ディレクトリを指定する。INITLIST は、A2.4 や A2.5 で用いたものと同様の初期日付リストファイルで、これが指定する初期日の予報データを次々に変換する。OUTDIR には変換した GrADS データの出力ディレクトリを指定する（この例では、作業ディレクトリにそのまま出力）。DATFILE には、変換データのファイル名を与える。MEMBERS には、予報のアンサンブルメンバー名のリストを与える。DIRFCSTP には、A2.5 の予報実験システムが出力した変換元 p-面データ (fcst_p.nus) が存在するディレクトリを指定する。#namelist parameters --- 以下は、変換プログラムに与えるネームリストの設定であり、この部分を編集することによって、変換する予報対象時刻や予報要素・レベルなどを指定することができる。ネームリストの詳細については A3.2 を参照されたい。

編集終了後、このシェルスクリプトを llsubmit 実行する（$BGMDIR/Tool ディレクトリで）：

```
$ llsubmit rdnus2gr_ens.sh
```

ジョブが終了すると、初期日付ごとに ${OUTDIR}/${DATFILE}.（日付） という名前の GrADS データファイルが出力される。なお、対応する GrADS 定義ファイルは自動生成されないので、別途用意する必要がある。（データファイルは、GrADS の通常のデータ配列

順 : 東西、南北、高度、対象時刻、メンバー　に従っている。）$BGMDIR/Tool/zuvtdo_ens.ctl は上記の例に対応した、初期日ごとの 1 データファイルに対応する GrADS 定義ファイルであり、これを参考にされたい。

A3 BGM 関連ツール

ここでは､BGM アンサンブル予報システムを用いた実験に関連して用いることのできる、各種関連ツールについて紹介する。これらのツールの実行シェルスクリプトなど各ファイルは、BGM 関連ツールディレクトリ $BGMDIR/Tool に用意されている。

A3.1 北半球 BGM 摂動データ → 熱帯（ダミー）摂動データの変換

A2.3 で述べた、熱帯 BGM サイクルの開始時刻用ダミーデータを北半球摂動データから変換して作成するツールである[10]。変換を行うシェルスクリプトファイルは cpptb.nh-tr.sh である。テキストエディタでこのファイルを開き、以下の部分を適宜編集する：

```
#--- set belows ------------------------------------------------------------
# user parameters on MRI-system
# (also edit #@account_no above)
GRP=cl
UER=syabu

HOMEDIR=/home3/${GRP}/${UER}       # (alias ; no need to edit)
WOMEDIR=/work/${GRP}/${UER}
SOMEDIR=/short/${GRP}/${UER}

BGMDIR=${HOMEDIR}/BGM                 # BGM system dir.
WRKDIR=${SOMEDIR}/BGM/temp/ptbtro   # working dir. !!! cleaned up at start !!!

DIRNH=${WOMEDIR}/BGM/Data/Ptbnh4/ptb12      # NH-Ptb. data directory (input)
DIRTR=${WOMEDIR}/BGM/Data/Ptbtro            # TR-Ptb. data directory (output)
YYYY=2004                                   # date    (year)
MM=01                                 #         (month)
DD=06                                 #         (day)
HH=12                                 #         (hour)
# ---------------------------------------------------------------------------
```

最初に、この前の部分にある @account_no= の行の課金番号を予め記入する。GRP, USR は MRI システムのユーザー情報、HOMEDIR から BGMDIR は、A2.2 までと同様。WRKDIR

[10]データ実体は変更せず、NuSDaS 種別 (type3) のみを変換する。

には、このデータ変換のための作業ディレクトリを指定する。DIRNH には、変換元の北半球摂動データが存在する(ptb12)ディレクトリを、DIRTR には、変換後の熱帯摂動データが作成されるディレクトリを、それぞれ指定する。YYYY, MM, DD, HH は、変換データの日付（西暦年、月、日、UTC 時刻）である。

編集終了後、llsubmit 実行する（$BGMDIR/Tool ディレクトリで）：

$ llsubmit cpptb.nh-tr.sh

ジョブが終了すると、${DIRTR}/（日付）/ptbtro_cycl12.nus という、熱帯摂動データが作成される。この ${DIRTR} を A2.3 の pre_tro.sh の P1STDIR= に指定すれば、熱帯 BGM サイクルが開始できる。

A3.2 NuSDaS → GrADS データ変換プログラム rdnus2gr

プログラム Rdnus2gr は、NuSDaS 形式データを GrADS 形式（４バイト実数）データに変換するプログラムである[11]。A2.6 ですでにこのプログラムを利用した予報 NuSDaS データの変換の実例を示したが、プログラムに与えるネームリストを変更することによって様々な変換・出力の指定が可能になっている。以下では、その設定項目について説明する。

ツールディレクトリにある、変換シェルスクリプト rdnus2gr_ens1.sh は、９メンバー予報の、３つの予報時間 FT＝0,24,48（時間）での 500hPa 高度、850hPa 気温、地上気圧、および前 24 時間降水量を、GrADS 形式データに変換する例である[12]。そのネームリスト設定部分は以下のようになっている：

```
# namelist parameters ---------------------------------------------------------
NAMGR="fname='temp.dat' ,xdef=288 ,ydef=145 ,zdef=1 ,tdef=1"
NAMSK="fmask='nomask' ,lvls=23 ,vlvl='SURF','1000','925 ','850 ','700 ','600 ','500 ','400 ','300
','250 ','200 ','150 ','100 ','70  ','50  ','30  ','20  ','10  ','7   ','5   ','3   ','2   ','1   '"
NAMVR="iznl=0  ,nvar=4  ,celm='Z       ','T       ','PSEA   ','RAIN   ' ,clvl='500  ','850
','SURF','SURF'"
#! idate is set in initdate loop
NAMDT0="idate=YYYY,MM,DD,HH,0 ,nkt=3,ikt=0,24,48"
#! member is set in member loop
NAMNS0="type1='_SF1LLPP' ,type2='FCSV' ,type3='STD1' ,member='MEMB'"
NAMGL="ig2l=0"
# -----------------------------------------------------------------------------
```

以下ネームリスト群ごとに説明する[13]。

---

[11] 他の同様の変換プログラムを利用できる方は、そちらを利用してよい。

[12] もちろん、FT=00 時の前 24 時間降水量は未定義。

[13] プログラム rdnus2gr の正規のネームリスト群名は、以下の説明順に NUMGRA, NUMMSK, NUMVAR, NAMIDT, NAMNUS および NAMG2L。ここでは代わりに、対応する変換シェルスクリプト上のシェル

NAMGR：出力する GrADS 形式データに関するネームリスト群

fname： 出力データファイル名

xdef, ydef： データの東西、南北格子数

（zdef, tdef：現在使用されないネームリスト、設定不要）

NAMSK：地形マスクに関する群

fmask： マスクファイル名（'nomask'を与えると、マスクファイル不使用）lvls： マスクファイルで指定している鉛直レベル数

vlvl： 各鉛直レベルの気圧 [hPa] （左詰め４文字）

※マスクファイルの詳細についてはここでは説明を省略。マスクファイルなし、で使用いただきますが、その場合でもネームリスト lvls と vlvl をプログラムは参照するので、これらはこのように指定しておくこと。

NAMVR：出力したい予報要素に関する群

nvar：（celm,clvl）の組の数

celm：予報要素名

clvl： レベル気圧

celm と clvl には、（要素名、レベル気圧）の組を nvar 個列記する。これらには A2.5 で説明した予報 p-面ファイルの要素名、気圧の中から左詰め文字列（それぞれ６文字と４文字）として与えること（脚注４）。また、clvl='ALL ' と設定することもでき、その場合は対応する要素（celm）は（NAMSK 群の vlvl の）全レベルについて変換される。

iznl：データの帯状平均処理の指定フラグ

（１を指定すると帯状平均値で出力する。そのとき、ydef=1。）

NAMDT0：変換データの対象時間についての群

idate： 初期日付（西暦年、月、日、UTC 時刻）

nkt：対象時間の個数

ikt：対象時間（初期時刻からのリードタイム[hr]）

ikt には、nkt 個の時間を列記する。また、nkt = 0 と指定することもでき、その場合は一定時間間隔ごとの対象時間指定が可能。例えば、216 時間後までの６時間ごとの各予報値を出力したい場合には、nkt=0, ikt=6,216,6 と記述することができる。（すなわち nkt が０のときの ikt には、始点時刻、終点時刻、時間間隔の３つを与える）。

NUMNS0：NuSDaS データに関する群

type1～3：NuSDaS 種別（本予報データの場合はこの例のように記述）[14]

member：アンサンブルメンバー名

（上記シェルでは変数 MEMB で９メンバーが予め指定されている。）

変数で表している。

[14] NuSDaS 種別は、どういうモデルの何に関する NuSDaS データかを示す指示符号群。

NAMGL：標準ガウス格子の NuSDaS データに対するネームリスト群
ig2l ：標準ガウスデータを緯度経度データに格子変換するフラグ
（=1 とすると変換、=0 は無変換）
p-面ファイルは等緯度経度データなので、無変換を指定する。

変換は、A2.6 の例と同じように、llsubmit で実行する。このネームリスト設定で変換された GrADS 形式データに対応した GrADS コントロールファイルは、ztpr_ens.ctl のようになる。

A3.3 JRA-25 再解析データの NuSDaS 形式化

第３章や A1.2 で述べたように、本実験システムの入力（解析/気候値）データは気象庁 NuSDaS 形式である必要がある。気象研究所の front1:/mri-data に配置されている JRA-25 / JCDAS データは GRIB (1) 形式であるため、本研究ではまず最初に GRIB から NuSDaS への形式変換が必要になった。GRIB 形式データを読み込める GrADS のバージョンを利用して、以下のように変換を行ったので[15]、ここにその概要を記しておく。

変換に用いたシェルスクリプトファイルは、データ期間によって以下を使い分けた：

jra25nus.sh : JRA-25 用（期間：1979～2004 年）
jcdasnus.-200710.sh : JCDAS 用（期間：2005 年１月～2007 年 10 月）
jcdasnus.200711-200804.sh : JCDAS 用（期間：2007 年 11 月～2008 年４月）
jcdasnus.200805-.sh : JCDAS 用（期間：2008 年５月～2012 年８月、
ただし 2010 年１月を除く）
jcdasnus.201001.sh : JCDAS 用（期間：2010 年１月）

これらのシェルを編集して実行すると、まず年・月（・日）ごとに、６時間値の対象 GRIB データを GrADS で読み込み、GrADS 形式で一旦出力する（生成される fwrite.gs という GrADS スクリプトをバッチ実行）。次いで、その GrADS 形式データを、A3.2 の Rdnus2gr の逆変換をするプログラム gr2nus.jra によって、NuSDaS 形式データに変換する、という２段階で処理を行った。上記のように JCDAS データに対しては複数の変換シェルが必要になったが、その理由は、この第一段階の変換で、/mri-data ディレクトリに GRIB データとともに配置されている GrADS 定義ファイルを利用した際に、定義ファイルの書き方がデータ期間によって異なり、その違いを考慮する必要があったためである。また、第２段階の NuSDaS 化においては、今回の BGM アンサンブルシステムへの入力として必要でない鉛直速度（OMG）などは変換しなかった。変換したデータは、以下のとおり（Q は比湿、その他の要素名は A2.5 を参照、sfc は地表面値の意味）：

PSEA, Z, U, V, T, TTD, CWC, Q, Usfc, Vsfc, Tsfc, TTDsfc, Qsfc

中間 GrADS 形式ファイルには各データはこの順に格納されていることを仮定して、後段の専用変換プログラム gr2nus.jra は動作する。（変換プログラムに与えるネームリストについ

[15]気象庁数値予報課の grib2nus ツールを用いた変換では不具合が生じたため。

ては、ソースファイル gr2nus.jra.f90 の冒頭部分のコメントを参照のこと。）

A3.4 陸面気候値データの解析データ形式化

第３章や A1.2 で述べたように、本実験システムの陸面データは、気象庁気候情報課のオフライン陸面解析から作成された気候値データであるが、システムの取扱い上の問題や、将来の解析値利用も考慮して、データは日付を持った解析値として扱っている。以下では、システムディスクの Data/lfin_lnd 以下の陸面“解析”データを作成した方法を記す。

プログラム setland.clim は、システム構築作業当初に気候情報課から提供された気候値データから形式上の解析値データを得るものである。シェルスクリプト setland.clm.sh は、閏日のない 365 日の lfin_lnd 形式気候値データ(00 および 12UTC、仮の年は cyear=2010）を読み込み、データ日付（年）を変更して別の NuSDaS データとして書き出す。なお、A2.1 の BGM プレサイクルを実行する際には、06 および 18UTC の陸面データも必要になるが、それぞれ 00,12UTC データで代用した。また、閏日（2/29）の陸面データについては、別のプログラム（cpland.clim (シェルスクリプト setland.clm.leapday.sh)）によって、2/28 データで代用する処理を行った。

シェルスクリプト setland.clm.sh において編集が必要なのは、DIRLAND= ： 気候値データの場所の指定、および、YYYY ループの出力年のリストの指定、などである。このスクリプトを実行すると、各年のデータが $WRKDIR/lfin_lnd の下に書き出される。閏日データを作成するシェルスクリプト setland.clm.leapday.sh は、365 日データを setland.clm.sh で作成した後に続けて、2010 年２月 28 日データが存在するディレクトリを DIRLAND に指定して実行するとよい（ループ YYYY で指定された、すでに存在する閏年のディレクトリに、２月 29 日分が追加作成される）。

Acknowledgement

We appreciate the generous technical support from members of the numerical forecast group of the Climate Prediction Division of the JMA. Mr. Noriyuki Adachi of the JMA helped us greatly with the implementation of the operational BGM cycle system of the JMA onto the MRI supercomputing system. Mr. Hitoshi Sato of JMA gave us much useful advice about the operational BGM cycle system of the JMA.

References

Adachi, Y., S. Yukimoto, M. Deushi, A. Obata, H. Nakano, T. Y. Tanaka, M. Hosaka, T. Sakami, H. Yoshimura, M. Hirabara, E. Shindo, H. Tsujino, R. Mizuta, S. Yabu, T. Koshiro, T. Ose, and A. Kitoh, 2013: Basic performance of a new earth system model of the Meteorological Research Institute (MRI-ESM1). *Pap. Meteor. Geophys.*, **64**, 1–19.

Buizza, R., M. J. Miller, and T. N. Palmer, 1999: Stochastic simulation of model uncertainties in the ECMWF ensemble prediction system. *Q. J. R. Meteorol. Soc.*, **125**, 2887-2908.

Buizza, R., Tribbia, J., Molteni, F., and Palmer, T. N., 1993: Computation of optimal unstable structures for a numerical weather prediction model. *Tellus*, **45A**, 388-407.

Chikamoto, Y., H. Mukougawa, T. Kubota, H. Sato, A. Ito, and S. Maeda, 2007: Evidence of growing bred vector associated with the tropical intraseasonal oscillation, *Geophys. Res. Lett.,* **34**, *L04806, doi:10.1029/2006GL028450.*

Dee D.P. *et al*. 2011: The ERA-Interim reanalysis: configuration and performance of the data assimilation system, *Q. J. R. Meteorol. Soc., 137,* 553-597, doi:10.1002/qj.828.

Endo, H., A. Kitoh, T. Ose, R. Mizuta, and S. Kusunoki, 2012: Future changes in Asian precipitation simulated by multi-physics and multi-sea surface temperature ensemble experiments with high-resolution Meteorological Research Institute atmospheric general circulation models (MRI-AGCMs). *J. Geophys. Res., 117, D16118,* doi:10.1029/2012JD017874.

Hirai, M., T. Sakashita, H. Kitagawa, T. Tsuyuki, M. Hosaka, and M. Oh'izumi, 2007: Development

and validation of a new land surface model for JMA's operational global model using the CEOP observation dataset. *J. Meteor. Soc. Japan, 85A*, 1–24.

Ishii, M., A. Shouji, S. Sugimoto and T. Matsumoto, 2005: Objective Analyses of Sea-Surface Temperature and Marine Meteorological Variables for the 20th Century Using ICOADS and the KOBE Collection. *Int. J. of Climatology*, **25**, 865-879.

Kawai, H., 2006: PDF cloud scheme and prognostic cloud scheme in JMA global model. *CAS/JSC WGNE Research Activities in Atmospheric and Ocean Modeling, 36,* 4.15–4.16.

Kyoda, M., 2000: Performance of weekly ensemble forecast system. NPD/JMA Technical Report, **47**, Numerical Prediction Division, Japan Meteorological Agency. ,86-93. (in Japanese)

Kyoda, M., 2006: Weekly ensemble forecast. NPD/JMA Technical Report, **52**, Numerical Prediction Division, Japan Meteorological Agency. ,23-33. (in Japanese)

Legras, B. and R. Vautard, 1995: A guide to Liapunov vectors. Proceedings of the ECMWF seminar on Predictability, 143-156.

Lorenz, E. N., 1963: Deterministic non-periodic flows. *J. Atmos. Sci.*, **20**, 130–141.

Mizuta, R., H. Yoshimura, H. Murakami, M. Matsueda, H. Endo, T. Ose, K. Kamiguchi, M. Hosaka, M. Sugi, S. Yukimoto, S. Kusunoki, and A. Kitoh, 2012: Climate simulations using MRI-AGCM3.2 with 20-km grid. *J. Meteor. Soc. Japan, 90A,* 233-258.

Mukougawa H., H. Sakai, and T. Hirooka, 2005: High sensitivity to the initial condition for the prediction of stratospheric sudden warming, *Geophys. Res. Lett.*, *32,* L17806, doi:10.1029/2005GL022920.

Murakami, H., and T. Matsumura, 2007: Development of an effective non-linear normal mode initialization method for a high resolution global model. *J. Meteor. Soc. Japan, 85,* 187-208.

Murakami, H., Y. Wang, H. Yoshimura, R. Mizuta, M. Sugi, E. Shindo, Y. Adachi, S. Yukimoto, M. Hosaka, S. Kusunoki, T. Ose, and A. Kitoh, 2011: Future changes in tropical cyclone activity projected by the new high-resolution MRI-AGCM. *J. Climate, 25,* 3237-3260.

Onogi, K., J.Tsutsui, H.Koide, M. Sakamoto, S. Kobayashi, H. Hatsushika, T. Matsumoto, N. Yamazaki, H. Kamahori, K. Takahashi, S. Kadokura, K. Wada, K. Kato, R. Oyama, T. Ose, N. Mannoji and R. Taira, 2007: The JRA-25 Reanalysis. *J. Meteor. Soc. Japan*, **85**, 369-432.

Sellers, P. J., Y. Mints, Y. C. Sud and A. Dalcher, 1986: A simple biosphere model (SiB) for use within general circulation models. *J. Atmos. Sci., 43,* 505-531.

Taylor, K. E., R. J. Stouffer, and G. A. Meehl, 2012: An overview of CMIP5 and the experiment design, *Bull. Am. Meteorol. Soc., 93,* 485–498, doi:10.1175/BAMS-D-11-00094.1.

Tiedtke, M., 1993: Representation of clouds in largescale models. *Mon. Wea. Rev., 121,* 3040–3061.

Toth, Z., and E. Kalnay, 1993: Ensemble forecasting at NMC: The generation of perturbations. *Bull. Amer. Meteor. Soc.*, **74**, 2317–2330.

Toth, Z., and E. Kalnay, 1997: Ensemble forecasting at NCEP and the breeding method. *Mon. Wea. Rev.*, **125**, 3297–3319.

Yamaguchi, M., R. Sakai, M. Kyoda, T. Komori, and T. Kadowaki, 2009: Typhoon Ensemble Prediction System developed at the Japan Meteorological Agency. *Mon. Wea. Rev.*, **137**, 2592–2604.

Yukimoto, S, H. Yoshimura, M. Hosaka, T. Sakami, H. Tsujino, M. Hirabara, T. Y. Tanaka, M. Deushi, A. Obata, H. Nakano, Y. Adachi, E. Shindo, S. Yabu, T. Ose and A. Kitoh, 2011: Meteorological Research Institute-Earth System Model v1 (MRIESM1) --Model description--. *Tech. Rep. Meteor. Res. Inst., 64,* 88 pp.

気象研究所技術報告一覧表

第 1 号　バックグラウンド大気汚染の測定法の開発（地球規模大気汚染特別研究班，1978）
Development of Monitoring Techniques for Global Background Air Pollution. (MRI Special Research Group on Global Atmospheric Pollution, 1978)

第 2 号　主要活火山の地殻変動並びに地熱状態の調査研究（地震火山研究部，1979）
Investigation of Ground Movement and Geothermal State of Main Active Volcanoes in Japan. (Seismology and Volcanology Research Division, 1979)

第 3 号　筑波研究学園都市に新設された気象観測用鉄塔施設（花房龍男，藤谷徳之助，伴野登，魚津博，1979）
On the Meteorological Tower and Its Observational System at Tsukuba Science City. (T. Hanafusa, T. Fujitani, N. Banno, and H. Uozu, 1979)

第 4 号　海底地震常時観測システムの開発（地震火山研究部，1980）
Permanent Ocean－Bottom Seismograph Observation System. (Seismology and Volcanology Research Division, 1980)

第 5 号　本州南方海域水温図－400m（又は 500m）深と 1,000m 深－（1934－1943 年及び 1954－1980 年）（海洋研究部，1981）
Horizontal Distribution of Temperature in 400m (or 500m) and 1,000m Depth in Sea South of Honshu, Japan and Western －North Pacific Ocean from 1934 to 1943 and from 1954 to 1980. (Oceanographical Research Division, 1981)

第 6 号　成層圏オゾンの破壊につながる大気成分及び紫外日射の観測（高層物理研究部，1982）
Observations of the Atmospheric Constituents Related to the Stratospheric ozon Depletion and the Ultraviolet Radiation. (Upper Atmosphere Physics Research Division, 1982)

第 7 号　83 型強震計の開発（地震火山研究部，1983）
Strong－Motion Seismograph Model 83 for the Japan Meteorological Agency Network. (Seismology and Volcanology Research Division, 1983)

第 8 号　大気中における雪片の融解現象に関する研究（物理気象研究部，1984）
The Study of Melting of Snowflakes in the Atmosphere. (Physical Meteorology Research Division, 1984)

第 9 号　御前崎南方沖における海底水圧観測（地震火山研究部・海洋研究部，1984）
Bottom Pressure Observation South off Omaezaki, Central Honsyu. (Seismology and Volcanology Research Division and Oceanographical Research Division, 1984)

第 10 号　日本付近の低気圧の統計（予報研究部，1984）
Statistics on Cyclones around Japan. (Forecast Research Division, 1984)

第 11 号　局地風と大気汚染質の輸送に関する研究（応用気象研究部, 1984）
Observations and Numerical Experiments on Local Circulation and Medium－Range Transport of Air Pollutions. (Applied Meteorology Research Division, 1984)

第 12 号　火山活動監視手法に関する研究（地震火山研究部，1984）
Investigation on the Techniques for Volcanic Activity Surveillance. (Seismology and Volcanology Research Division, 1984)

第 13 号　気象研究所大気大循環モデル－Ⅰ（MRI・GCM－Ⅰ）（予報研究部，1984）
A Description of the MRI Atmospheric General Circulation Model (The MRI・GCM－Ⅰ). (Forecast Research Division, 1984)

第 14 号　台風の構造の変化と移動に関する研究－台風 7916 の一生－（台風研究部，1985）
A Study on the Changes of the Three - Dimensional Structure and the Movement Speed of the Typhoon through its Life Time. (Typhoon Research Division, 1985)

第 15 号　波浪推算モデル MRI と MRI－Ⅱの相互比較研究－計算結果図集－（海洋気象研究部，1985）
An Intercomparison Study between the Wave Models MRI and MRI－Ⅱ －A Compilation of Results－ (Oceanographical Research Division, 1985)

第 16 号　地震予知に関する実験的及び理論的研究（地震火山研究部，1985）
Study on Earthquake Prediction by Geophysical Method. (Seismology and Volcanology Research Division, 1985)

第 17 号　北半球地上月平均気温偏差図（予報研究部，1986）
Maps of Monthly Mean Surface Temperature Anomalies over the Northern Hemisphere for 1891－1981. (Forecast Research Division, 1986)

第 18 号　中層大気の研究（高層物理研究部, 気象衛星研究部, 予報研究部, 地磁気観測所，1986）
Studies of the Middle Atmosphere. (Upper Atmosphere Physics Research Division, Meteorological Satellite Research Division, Forecast Research Division, MRI and the Magnetic Observatory, 1986)

第 19 号　ドップラーレーダによる気象・海象の研究（気象衛星研究部・台風研究部・予報研究部・応用気象研究部・海洋研究部，1986）
Studies on Meteorological and Sea Surface Phenomena by Doppler Radar. (Meteorological Satellite Research Division, Typhoon Research Division, Forecast Research Division, Applied Meteorology Research Division, and Oceanographical Research Division, 1986)

第 20 号　気象研究所対流圏大気大循環モデル（MRI・GCM－Ⅰ）による 12 年間分の積分（予報研究部，1986）
Mean Statistics of the Tropospheric MRI・GCM－Ⅰbased on 12－year Integration. (Forecast Research Division, 1986)

第 21 号　宇宙線中間子強度 1983－1986（高層物理研究部，1987）
Multi－Directional Cosmic Ray Meson Intensity 1983－1986. (Upper Atmosphere Physics Research Division, 1987)

第 22 号　静止気象衛星「ひまわり」画像の噴火噴煙データに基づく噴火活動の解析に関する研究（地震火山研究部，1987）
Study on Analysis of Volcanic Eruptions based on Eruption Cloud Image Data obtained by the Geostationary Meteorological satellite (GMS). (Seismology and Volcanology Research Division, 1987)
第 23 号　オホーツク海海洋気候図（篠原吉雄，四竈信行，1988）
Marine Climatological Atlas of the sea of Okhotsk. (Y. Shinohara and N. Shikama, 1988)
第 24 号　海洋大循環モデルを用いた風の応力異常に対する太平洋の応答実験（海洋研究部，1989）
Response Experiment of Pacific Ocean to Anomalous Wind Stress with Ocean General Circulation Model. (Oceanographical Research Division, 1989)
第 25 号　太平洋における海洋諸要素の季節平均分布（海洋研究部，1989）
Seasonal Mean Distribution of Sea Properties in the Pacific. (Oceanographical Research Division, 1989)
第 26 号　地震前兆現象のデータベース（地震火山研究部, 1990）
Database of Earthquake Precursors. (Seismology and Volcanology Research Division, 1990)
第 27 号　沖縄地方における梅雨期の降水システムの特性（台風研究部，1991）
Characteristics of Precipitation Systems During the Baiu Season in the Okinawa Area. (Typhoon Research Division, 1991)
第 28 号　気象研究所・予報研究部で開発された非静水圧モデル（猪川元興・斉藤和雄，1991）
Description of a Nonhydrostatic Model Developed at the Forecast Research Department of the MRI. (M. Ikawa and K. Saito, 1991)
第 29 号　雲の放射過程に関する総合的研究（気候研究部・物理気象研究部・応用気象研究部・気象衛星・観測システム研究部・台風研究部，1992）
A Synthetic Study on Cloud－Radiation Processes. (Climate Research Department, Physical Meteorology Research Department, Applied Meteorology Research Department, Meteorological Satellite and Observation System Research Department, and Typhoon Research Department, 1992)
第 30 号　大気と海洋・地表とのエネルギー交換過程に関する研究（三上正男・遠藤昌宏・新野　宏・山崎孝治，1992）
Studies of Energy Exchange Processes between the Ocean－Ground Surface and Atmosphere. (M. Mikami, M. Endoh, H. Niino, and K. Yamazaki, 1992)
第 31 号　降水日の出現頻度からみた日本の季節推移－30 年間の日降水量資料に基づく統計－（秋山孝子，1993）
Seasonal Transition in Japan, as Revealed by Appearance Frequency of Precipitating-Days. －Statistics of Daily Precipitation Data During 30 Years－(T. Akiyama, 1993)
第 32 号　直下型地震予知に関する観測的研究（地震火山研究部，1994）
Observational Study on the Prediction of Disastrous Intraplate Earthquakes. (Seismology and Volcanology Research Department, 1994)
第 33 号　各種気象観測機器による比較観測（気象衛星・観測システム研究部，1994）
Intercomparisons of Meteorological Observation Instruments. (Meteorological Satellite and Observation System Research Department, 1994)
第 34 号　硫黄酸化物の長距離輸送モデルと東アジア地域への適用（応用気象研究部，1995）
The Long－Range Transport Model of Sulfur Oxides and Its Application to the East Asian Region. (Applied Meteorology Research Department, 1995)
第 35 号　ウインドプロファイラーによる気象の観測法の研究（気象衛星・観測システム研究部，1995）
Studies on Wind Profiler Techniques for the Measurements of Winds. (Meteorological Satellite and Observation System Research Department, 1995)
第 36 号　降水・落下塵中の人工放射性核種の分析法及びその地球化学的研究（地球化学研究部，1996）
Geochemical Studies and Analytical Methods of Anthropogenic Radionuclides in Fallout Samples. (Geochemical Research Department, 1996)
第 37 号　大気と海洋の地球化学的研究（1995 年及び 1996 年）（地球化学研究部，1998）
Geochemical Study of the Atmosphere and Ocean in 1995 and 1996. (Geochemical Research Department, 1998)
第 38 号　鉛直２次元非線形問題（金久博忠，1999）
Vertically 2-dmensional Nonlinear Problem (H. Kanehisa, 1999)
第 39 号　客観的予報技術の研究（予報研究部，2000）
Study on the Objective Forecasting Techniques（Forecast Research Department, 2000）
第 40 号　南関東地域における応力場と地震活動予測に関する研究（地震火山研究部，2000）
Study on Stress Field and Forecast of Seismic Activity in the Kanto Region（Seismology and Volcanology Research Department, 2000）
第 41 号　電量滴定法による海水中の全炭酸濃度の高精度分析および大気中の二酸化炭素と海水中の全炭酸の放射性炭素同位体比の測定（石井雅男・吉川久幸・松枝秀和，2000）
Coulometric Precise Analysis of Total Inorganic Carbon in Seawater and Measurements of Radiocarbon for the Carbon Dioxide in the Atmosphere and for the Total Inorganic Carbon in Seawater（I.Masao, H.Y.Inoue and H.Matsueda, 2000）
第 42 号　気象研究所／数値予報課統一非静力学モデル（斉藤和雄・加藤輝之・永戸久喜・室井ちあし，2001）
Documentation of the Meteorological Research Institute / Numerical Prediction Division Unified Nonhydrostatic Model (Kazuo Saito, Teruyuki Kato, Hisaki Eito and Chiashi Muroi，2001)
第 43 号　大気および海水中のクロロフルオロカーボン類の精密測定と気象研究所クロロフルオロカーボン類標準ガスの確立（時枝隆之・井上(吉川)久幸，2004）
Precise measurements of atmospheric and oceanic chlorofluorocarbons and MRI chlorofluorocarbons calibration scale

(Takayuki Tokieda and Hisayuki Y. Inoue，2004)

第 44 号　PostScript コードを生成する描画ツール"PLOTPS"マニュアル（加藤輝之，2004）
Documentation of "PLOTPS": Outputting Tools for PostScript Code (Teruyuki Kato，2004)

第 45 号　気象庁及び気象研究所における二酸化炭素の長期観測に使用された標準ガスのスケールとその安定性の再評価に関する調査・研究（松枝秀和・須田一人・西岡佐喜子・平野礼朗・澤　庸介・坪井一寛・堤　之智・神谷ひとみ・根本和宏・長井秀樹・吉田雅司・岩野園城・山本　治・森下秀昭・鎌田匡俊・和田　晃，2004）
Re-evaluation for scale and stability of CO_2 standard gases used as long-term observations at the Japan Meteorological Agency and the Meteorological Research Institute (Hidekazu Matsueda, Kazuto Suda, Sakiko Nishioka, Toshirou Hirano, Yousuke, Sawa, Kazuhiro Tuboi, Tsutumi, Hitomi Kamiya, Kazuhiro Nemoto, Hideki Nagai, Masashi Yoshida, Sonoki Iwano, Osamu Yamamoto, Hideaki Morishita, Kamata, Akira Wada，2004)

第 46 号　地震発生過程の詳細なモデリングによる東海地震発生の推定精度向上に関する研究（地震火山研究部，2005）
A Study to Improve Accuracy of Forecasting the Tokai Earthquake by Modeling the Generation Processes (Seismology and Volcanology Research Department, 2005)

第 47 号　気象研究所共用海洋モデル（MRI.COM）解説（海洋研究部，2005）
Meteorological Research Institute Community Ocean Model (MRI.COM) Manual (Oceanographical Research Department, 2005)

第 48 号　日本海降雪雲の降水機構と人工調節の可能性に関する研究（物理気象研究部・予報研究部，2005）
Study of Precipitation Mechanisms in Snow Clouds over the Sea of Japan and Feasibility of Their Modification by Seeding (Physical Meteorology Research Department, Forecast Research Department, 2005)

第 49 号　2004 年日本上陸台風の概要と環境場（台風研究部, 2006）
Summary of Landfalling Typhoons in Japan, 2004 (Typhoon Research Department, 2006)

第 50 号　栄養塩測定用海水組成標準の 2003 年国際共同実験報告（青山道夫，2006）
2003 Intercomparison Exercise for Reference Material for Nutrients in Seawater in a Seawater Matrix (Michio Aoyama, 2006)

第 51 号　大気および海水中の超微量六フッ化硫黄(SF_6)の測定手法の高度化と SF_6 標準ガスの長期安定性の評価（時枝隆之、石井雅男、斉藤 秀、緑川 貴, 2007）
Highly developed precise analysis of atmospheric and oceanic sulfur hexafluoride (SF_6) and evaluation of SF_6 standard gas stability (Takayuki Tokieda, Masao Ishii, Shu Saito and Takashi Midorikawa, 2007)

第 52 号　地球温暖化による東北地方の気候変化に関する研究（仙台管区気象台, 環境・応用気象研究部, 2008）
Study of Climate Change over Tohoku District due to Global Warming (Sendai District Meteorological Observatory, Atmospheric Environment and Applied Meteorology Research Department, 2008)

第 53 号　火山活動評価手法の開発研究（地震火山研究部, 2008）
Studies on Evaluation Method of Volcanic Activity (Seismology and Volcanology Research Department, 2008)

第 54 号　日本における活性炭冷却捕集およびガスクロ分離による気体計数システムによる ^{85}Kr の測定システムの構築および 1995 年から 2006 年の測定結果（青山道夫, 藤井憲治, 廣瀬勝己, 五十嵐康人, 磯貝啓介, 新田 済, Hartmut Sartorius, Clemens Schlosser, Wolfgang Weiss, 2008）
Establishment of a cold charcoal trap-gas chromatography-gas counting system for ^{85}Kr measurements in Japan and results from 1995 to 2006 (Michio Aoyama, Kenji Fujii, Katsumi Hirose, Yasuhito Igarashi, Keisuke Isogai, Wataru Nitta, Hartmut Sartorius, Clemens Schlosser, Wolfgang Weiss, 2008)

第 55 号　長期係留による 4 種類の流速計観測結果の比較（中野俊也, 石崎 廣, 四竈信行, 2008）
Comparison of Data from Four Current Meters Obtained by Long-Term Deep-Sea Moorings (Toshiya Nakano, Hiroshi Ishizaki and Nobuyuki Shikama, 2008)

第 56 号　CMIP3 マルチモデルアンサンブル平均を利用した将来の海面水温・海氷分布の推定（水田 亮, 足立恭将, 行本誠史, 楠 昌司, 2008）
Estimation of the Future Distribution of Sea Surface Temperature and Sea Ice Using the CMIP3 Multi-model Ensemble Mean (Ryo Mizuta, Yukimasa Adachi, Seiji Yukimoto and Shoji Kusunoki, 2008)

第 57 号　閉流路中のフローセルを用いた分光光度法自動分析装置による海水の高精度 pH_T 測定（斉藤 秀, 石井雅男, 緑川 貴, 井上（吉川）久幸, 2008）
Precise Spectrophotometric Measurement of Seawater pH_T with an Automated Apparatus using a Flow Cell in a Closed Circuit（Shu Saito, Masao Ishii, Takashi Midorikawa and Hisayuki Y. Inoue, 2008）

第58号　栄養塩測定用海水組成標準の2006年国際共同実験報告（青山道夫,J. Barwell-Clarke, S. Becker, M. Blum, Braga E.S., S. C. Coverly, E. Czobik, I. Dahllöf, M. Dai, G. O Donnell, C. Engelke, Gwo-Ching Gong, Gi-Hoon Hong, D. J. Hydes, Ming-Ming Jin, 葛西広海, R. Kerouel, 清本容子, M. Knockaert, N. Kress, K. A. Krogslund, 熊谷正光, S. Leterme, Yarong Li, 増田真次, 宮尾 孝, T. Moutin, 村田昌彦, 永井直樹, G. Nausch, A. Nybakk, M. K. Ngirchechol, 小川浩史, J. van Ooijen, 太田秀和, J. Pan, C. Payne, O. Pierre-Duplessix, M. Pujo-Pay, T. Raabe, 齊藤一浩, 佐藤憲一郎, C. Schmidt, M. Schuett, T. M. Shammon, J. Sun, T. Tanhua, L. White, E.M.S. Woodward, P. Worsfold, P. Yeats, 芳村 毅, A. Youénou, Jia-Zhong Zhang, 2008）
2006 Inter-laboratory Comparison Study for Reference Material for Nutrients in Seawater（M. Aoyama, J. Barwell-Clarke, S. Becker, M. Blum, Braga E. S., S. C. Coverly, E. Czobik, I. Dahllöf, M. H. Dai, G. O. Donnell, C. Engelke, G. C. Gong, Gi-Hoon Hong, D. J. Hydes, M. M. Jin, H. Kasai, R. Kerouel, Y. Kiyomono, M. Knockaert, N. Kress, K. A. Krogslund, M. Kumagai, S. Leterme, Yarong Li, S. Masuda, T. Miyao, T. Moutin, A. Murata, N. Nagai, G. Nausch, M. K. Ngirchechol, A. Nybakk, H. Ogawa, J. van Ooijen, H. Ota, J. M. Pan, C. Payne, O. Pierre-Duplessix, M. Pujo-Pay, T. Raabe, K. Saito, K. Sato, C. Schmidt, M. Schuett, T. M. Shammon, J. Sun, T. Tanhua, L. White, E.M.S. Woodward, P. Worsfold, P. Yeats, T.

Yoshimura, A. Youénou, J. Z. Zhang, 2008）

第 59 号　気象研究所共用海洋モデル(MRI.COM)第 3 版解説（辻野博之, 本井達夫, 石川一郎, 平原幹俊, 中野英之, 山中吾郎, 安田珠幾, 石崎廣（気象研究所海洋研究部）, 2010）

Reference manual for the Meteorological Research Institute Community Ocean Model (MRI.COM) Version 3（Hiroyuki Tsujino, Tatsuo Motoi, Ichiro Ishikawa, Mikitoshi Hirabara, Hideyuki Nakano, Goro Yamanaka, Tamaki Yasuda, and Hiroshi Ishizaki (Oceanographic Research Department), 2010）

第 60 号　栄養塩測定用海水組成標準の 2008 年国際共同実験報告（青山道夫, Carol Anstey, Janet Barwell-Clarke, François Baurand, Susan Becker, Marguerite Blum, Stephen C. Coverly, Edward Czobik, Florence D'amico, Ingela Dahllöf, Minhan Dai, Judy Dobson, Magali Duval, Clemens Engelke, Gwo-Ching Gong, Olivier Grosso, 平山篤史, 井上博敬, 石田雄三, David J. Hydes, 葛西広海, Roger Kerouel, Marc Knockaert, Nurit Kress, Katherine A. Krogslund, 熊谷正光, Sophie C. Leterme, Claire Mahaffey, 光田均, Pascal Morin, Thierry Moutin, Dominique Munaron, 村田昌彦, Günther Nausch, 小川浩史, Jan van Ooijen, Jianming Pan, Georges Paradis, Chris Payne, Olivier Pierre-Duplessix, Gary Prove, Patrick Raimbault, Malcolm Rose, 齊藤一浩, 斉藤宏明, 佐藤憲一郎, Cristopher Schmidt, Monika Schütt, Theresa M. Shammon, Solveig Olafsdottir, Jun Sun, Toste Tanhua, Sieglinde Weigelt-Krenz, Linda White, E. Malcolm. S. Woodward, Paul Worsfold, 芳村毅, Agnès Youénou, Jia-Zhong Zhang, 2010）

2008 Inter-laboratory Comparison Study of a Reference Material for Nutrients in Seawater（青山道夫, Carol Anstey, Janet Barwell-Clarke, François Baurand, Susan Becker, Marguerite Blum, Stephen C. Coverly, Edward Czobik, Florence D'amico, Ingela Dahllöf, Minhan Dai, Judy Dobson, Magali Duval, Clemens Engelke, Gwo-Ching Gong, Olivier Grosso, 平山篤史, 井上博敬, 石田雄三, David J. Hydes, 葛西広海, Roger Kerouel, Marc Knockaert, Nurit Kress, Katherine A. Krogslund, 熊谷正光, Sophie C. Leterme, Claire Mahaffey, 光田均, Pascal Morin, Thierry Moutin, Dominique Munaron, 村田昌彦, Günther Nausch, 小川浩史, Jan van Ooijen, Jianming Pan, Georges Paradis, Chris Payne, Olivier Pierre-Duplessix, Gary Prove, Patrick Raimbault, Malcolm Rose, 齊藤一浩, 斉藤宏明, 佐藤憲一郎, Cristopher Schmidt, Monika Schütt, Theresa M. Shammon, Solveig Olafsdottir, Jun Sun, Toste Tanhua, Sieglinde Weigelt-Krenz, Linda White, E. Malcolm. S. Woodward, Paul Worsfold, 芳村毅, Agnès Youénou, Jia-Zhong Zhang, 2010）

第 61 号　強雨をもたらす線状降水帯の形成機構等の解明及び降水強度・移動速度の予測に関する研究（大阪管区気象台・彦根地方気象台・京都地方気象台・奈良地方気象台・和歌山地方気象台・神戸海洋気象台・松江地方気象台・鳥取地方気象台・舞鶴海洋気象台・広島地方気象台・徳島地方気象台・予報研究部, 2010）

Studies on formation process of line-shaped rainfall systems and predictability of rainfall intensity and moving speed（Osaka District Meteorological Observatory, Hikone Local Meteorological Observatory, Kyoto Local Meteorological Observatory, Nara Local Meteorological Observatory, Wakayama Local Meteorological Observatory, Kobe Marine Observatory, Matsue Local Meteorological Observatory, Tottori Local Meteorological Observatory, Maizuru Marine Observatory, Hiroshima Local Meteorological Observatory, Tokushima Local Meteorological Observatory AND Forecast Research Department, 2010）

第 62 号　WWRP 北京オリンピック 2008 予報実証/研究開発プロジェクト（齊藤和雄, 國井勝, 原昌弘, 瀬古弘, 原旅人, 山口宗彦, 三好建正, 黄偉健, 2010）

WWRP Beijing Olympics 2008 Forecast Demonstration/Research and Development Project (B08FDP/RDP)（Kazuo Saito, Masaru Kunii, Masahiro Hara, Hiromu Seko, Tabito Hara, Munehiko Yamaguchi, Takemasa Miyoshi and Wai-kin Wong, 2010）

第 63 号　東海地震の予測精度向上及び東南海・南海地震の発生準備過程の研究（地震火山研究部, 2011）

Improvement in prediction accuracy for the Tokai earthquake and research of the preparation process of the Tonankai and the Nankai earthquakes (Seismology and Volcanology Research Department, 2011)

第 64 号　気象研究所地球システムモデル第 1 版（MRI-ESM1）―モデルの記述―（行本誠史, 吉村裕正, 保坂征宏, 坂見智法, 辻野博之, 平原幹俊, 田中泰宙, 出牛真, 小畑淳, 中野英之, 足立恭将, 新藤永樹, 鍬将吉, 尾瀬智昭, 鬼頭昭雄, 2011）

Meteorological Research Institute-Earth System Model Version 1 (MRI-ESM1) — Model Description — (Seiji Yukimoto, Hiromasa Yoshimura, Masahiro Hosaka, Tomonori Sakami, Hiroyuki Tsujino, Mikitoshi Hirabara, Taichu Y. Tanaka, Makoto Deushi, Atsushi Obata, Hideyuki Nakano, Yukimasa Adachi, Eiki Shindo, Shoukichi Yabu, Tomoaki Ose and Akio Kitoh, 2011)

第 65 号　東南アジア地域の気象災害軽減国際共同研究（斉藤和雄, 黒田徹, 林修吾, 瀬古弘, 國井勝, 小司禎教, 上野充, 川畑拓矢, 余田成男, 大塚成徳, Nurjanna Joko Trilaksono, 許智揚, 古関俊也, Le Duc, Kieu Thi Xin, 黄偉健, Krushna Chandra Gouda, 2011）

International Research for Prevention and Mitigation of Meteorological Disasters in Southeast Asia (Kazuo Saito, Tohru Kuroda, Syugo Hayashi, Hiromu Seko, Masaru Kunii, Yoshinori Shoji, Mitsuru Ueno, Takuya Kawabata, Shigeo Yoden, Shigenori Otsuka, Nurjanna Joko Trilaksono, Tieh-Yong Koh, Syunya Koseki, Le Duc, Kieu Thi Xin, Wai-Kin Wong and Krushna Chandra Gouda, 2011)

第 66 号　太平洋における大気－海洋間二酸化炭素フラックス推定手法（杉本裕之, 平石直孝, 石井雅男, 緑川貴, 2012）

A method for estimating the sea-air CO2 flux in the Pacific Ocean (Hiroyuki Sugimoto, Naotaka Hiraishi, Masao Ishii and Takashi Midorikawa, 2012)

第 67 号　太平洋における大気－海洋間二酸化炭素フラックス推定手法（坪井一寛, 松枝秀和, 澤庸介, 丹羽洋介, 中村雅道, 久保池大輔, 岩坪昇平, 齊藤和幸, 花宮義和, 辻健太郎, 大森英裕, 西秀紘, 2012）

Development of a flask sampling and its high-precision measuring system for greenhouse gases observations using a cargo aircraft C-130H (Kazuhiro Tsuboi, Hidekazu Matsueda, Yousuke Sawa, Yosuke Niwa Masamichi Nakamura, Daisuke

Kuboike, Shohei Iwatsubo, Kazuyuki Saito Yoshikazu Hanamiya, Kentaro Tsuji, Hidehiro Ohmori, Hidehiro Nishi, 2012)

第 68 号　国際シンポジウム 電子顕微鏡を用いたエアロゾル研究（五十嵐康人, Weijun Li, Peter.R.Buseck, 岡田菊雄, 張代洲, 足立光司, 藤谷雄二, 嶋寺光, 五藤大輔, 三井千珠, 野島雅, 大島長, 松井仁志, 石元裕史, 松木篤, Pradeep Khatri, 中山智喜, 向井将平, 大石乾詞, 間山憲仁, 坂本哲夫, 直江寛明, 財前祐二, 塩流水洋樹, 田中泰宙, 梶野瑞王, 2013）

International Symposium on Aerosol Studies Explored by Electron Microscopy (Yasuhito Igarashi, Weijun Li, Peter. R. Buseck, Kikuo Okada, Daizhou Zhang, Kouji Adachi, Yuji Fujitani, Hikari Shimadera, Daisuke Goto, Chizu Mitsui, Masashi Nojima, Naga Oshima, Hitoshi Matsui, Hiroshi Ishimoto, Atsushi Matsuki, Pradeep Khatri, Tomoki Nakayama, Shohei Mukai, Kenji Ohishi, Norihito Mayama, Tetsuo Sakamoto, Hiroaki Naoe, Yuji Zaizen, Hiroki Shiozuru, Taichu Y. Tanaka and Mizuo Kajino, 2013)

第 69 号　マグマ活動の定量的把握技術の開発とそれに基づく火山活動度判定の高度化に関する研究（地震火山研究部, 2013）

Development of Quantitative Detection Techniques of Magma Activity and Improvement of Evaluation of Volcanic Activity Level (Seismology and Volcanology Research Department, MRI, 2013)

第 70 号　平成 23 年（2011 年）東北地方太平洋沖地震による津波高の現地調査報告（林豊，前田憲二，対馬弘晃，岡田正實，木村一洋，岩切一宏, 2013）

Reports on Field Surveys of Tsunami Heights from the 2011 off the Pacific Coast of Tohoku Earthquake (Yutaka Hayashi, Kenji Maeda, Hiroaki Tsushima, Masami Okada, Kazuhiro Kimura and Kazuhiro Iwakiri, 2013)

気象研究所技術報告は，1978（昭和53）年の初刊以来,気象研究所が必要の都度発行する刊行物であり，気象研究所の研究計画に基づき実施した研究に関する手法、データ、結果等についてのまとめ、または、すでに公表した研究論文類をとりまとめ総合的報告としたものを掲載する。

気　象　研　究　所　技　術　報　告　　ISSN 0386-4049
第　71　号

平成26年3月　発行

編集兼
発行者　気　象　研　究　所
〒305-0052　茨城県つくば市長峰１－１
TEL(029)853-8535

印　刷　者　朝日印刷株式会社　つくば支社
〒305-8519　茨城県つくば市東2-11-15
TEL(029)851-1188